

Analysis of the Hydrogen Embrittlement Susceptibility of Industrial Zn-Ni Brush Plating Process

Ashkan Arab

A thesis

in

The Department

of

Mechanical, Industrial and Aerospace engineering

Presented in Partial Fulfillment of Requirements

for the Degree of the Master of Applied Science (Mechanical Engineering) at

Concordia University Montréal, Québec, Canada

October 2022

© Ashkan Arab, 2022

Concordia University

School of Graduate studies

This is to certify that the thesis prepared

By: Ashkan Arab

Entitled: Analysis of the Hydrogen Embrittlement Susceptibility of Industrial Zn-Ni Brush Plating Process

and submitted in partial fulfillment of the requirements for the degree of

Master of Applied Science (Mechanical Engineering)

Complies with the regulations of the university and meets the accepted standards with respect to originality and quality.

Signed by the final examining committee:

<hr/>	Chair
Dr. Martin Pugh	
<hr/>	Examiner
Dr. Martin Pugh	
<hr/>	Examiner
Dr. Farjad Shadmehri	
<hr/>	Supervisor
Dr. Mamoun Medraj	

Approved by

 Graduate Program director
Dr. Sivakumar Narayanswamy

11/ 17/ 2022
Month/ Day/ Year

Dr. Mourad Debbabi
Dean, Gina Cody school of engineering and computer science

Abstract

Analysis of the Hydrogen Embrittlement Susceptibility of Industrial Zn-Ni Brush Plating Process

Ashkan Arab

In the present research, the hydrogen embrittlement (HE) susceptibility of an industrial Zinc-Nickel (Zn-Ni) brush plating process was investigated according to the ASTM F519 standard. Plated notched round bar samples were subjected to 200 h long sustained load test (SLT) to evaluate the HE susceptibility of the plating process. The results of the SLT indicated significant embrittlement in the absence of baking. However, baking for 24 h at 190°C according to industry standards relieved embrittlement completely. In addition, it was found that baking at a significantly lower temperature of 100°C relieved embrittlement as well. Change in plating parameters also failed to mitigate HE as samples plated at various current densities fractured in a similarly catastrophic manner under the SLT test. However, it was shown that by avoiding sandblasting in the pre-plating sample preparation stage, the results of the SLT improve significantly. Samples without sandblasting passed the SLT while those sandblasted failed after 11 h only. Another important finding was the outward diffusion of hydrogen at room temperature. This was shown by the fact that samples similar to those which failed the SLT managed to pass after being kept at room temperature for a week. The fracture surfaces of the embrittled samples showed intergranular fracture features at the crack initiation point and dimples and voids throughout the rest of the surface but the presence and visibility of these features varied among different samples.

Acknowledgements

I would like to express my sincere gratitude and appreciation to my thesis supervisor Dr. Mamoun Medraj for his support and encouragement during my M.A.Sc project.

Likewise, I would also like to thank Dr. Rajwinder Singh for his suggestions and guidance during this project. I am also sincerely grateful to Safran Landing Systems and specifically Mr. Alan Caceres for providing the necessary equipment for the experiments of this project. I would also like to thank my fellow TMG group members for their help throughout this journey.

Finally, I gratefully thank my family for their unwavering support and encouragement without which I could not have completed this project.

Table of contents

Table of Figures	VII
List of Tables	X
Chapter 1 : Introduction	1
1-1 Fundamental concepts of hydrogen embrittlement	2
1-2 Hydrogen in Metal Structure	3
1-2-1 Absorption into Metal Structure	3
1-2-2 Hydrogen Traps	4
1-3 Problem statement	5
1-4 Thesis layout.....	6
Chapter 2 : Literature review	7
2-1 Hydrogen embrittlement evaluation and characterization methods	8
2-2 Mechanisms of hydrogen embrittlement	9
2-2-1 Hydrogen Enhanced De-Cohesion (HEDE)	9
2-2-2 Hydrogen enhanced localized plasticity	10
2-2-3 Interaction and synergy of various hydrogen embrittlement mechanisms	11
2-5 Zn-Ni electro-plating	13
2-4 Hydrogen embrittlement in Zn-Ni and Cd electro-plated coatings	15
2-5 Brush plating.....	19
2-6 Research objectives	21
Chapter 3 : Experimental Procedure	22
3-1 Sample material	23
3-3 Plating procedure	26
3-3-1 Introduction to brush plating.....	26
3-3-2 Pre-plating preparations and sandblasting	28
3-3-3 Plating parameters.....	29
3-4 Sustained load test (SLT) for hydrogen embrittlement evaluation.....	32

3-4-1 Test equipment and considerations	32
3-4-2 Evaluation of the sustained load test results	33
Chapter 4 : Results and Discussion.....	35
4-1 Results of the sustained load test.....	36
4-1-1 Analysis of the sustained load test results.....	39
4-1-2 Coating morphology and characteristics.....	41
4-1-3 The effect of sandblasting.....	44
4-2 Fracture surface analysis	49
Chapter 5 : Conclusions and future directions.....	54
5-1 Conclusions	55
5-1-1 Conclusions derived from HE evaluation	55
5-1-2 Conclusions derived from microscopic observations of the fracture surfaces	55
5-1-3 Conclusions from secondary observations.....	56
5-2 Future directions	56
5-3 Contributions	57
References.....	58

Table of Figures

Figure 1-1 Interstitial sites (octahedral (O) sites and tetrahedral (T) sites) in FCC, HCP and BCC lattices [8].....	3
Figure 1-2 Schematic illustration of hydrogen traps sites [11].....	4
Figure 2-1 schematic illustration of HEDE mechanism showing the separation of atoms due to interatomic bonds by (i) presence of hydrogen in the lattice structure (ii) hydrogen being dissolved and (iii) presence of hydrogen at particle-matrix interfaces [48]	10
Figure 2-2 Schematic illustration of HELP mechanism demonstrating the coalescence of microvoids and plasticity being localized in areas of high hydrogen concentration [48].....	10
Figure 2-3 a) Fracture surface of the uncharged sample showing ductile fracture initiating at the notch b) Fracture surface of the charged sample showing intergranular fracture initiating ahead of the notch [53].....	12
Figure 2-4 Zn-Ni phase diagram [63]	13
Figure 2-5 Electro-deposited Zn-Ni coating with 8.5% Ni at a current density of 5mA/cm ² [64]	14
Figure 2-6 Electro-deposited Zn-Ni coating with 14% Ni at a current density of 5mA/cm ² [64]	14
Figure 2-7 Zn-Ni coating deposited at a) 48 mA/cm ² and b) 30 mA/cm ² [65]	15
Figure 2-8 SEM micrograph of Zn-Ni coating deposited at 15 mA/cm ² with 14% Ni [59].....	15
Figure 2-9 Permeation current density plotted against time for both Zn-Ni and Cd coatings [71]	16
Figure 2-10 Hydrogen permeation current transient for the Zn-Ni coatings plated at 30A/cm ² and 48A/cm ² [65].....	18
Figure 2-11 SEM surface morphology of Ni/nano-Al ₂ O ₃ composite coating: (a) automatically plated and (b) manually plated [81]	20
Figure 3-1 SEM image of the microstructure of the samples used in this research.....	24
Figure 3-2 Layout of type 1a.1 sample (dimension are in mm) [26].....	25
Figure 3-3 SEM image of an as-received test sample.....	25
Figure 3-4 SEM image of the notch of an as-received test sample	25
Figure 3-5 Schematic representation of the brush plating setup [86]	26
Figure 3-6 Rectifier used for brush plating.....	27

Figure 3-7 Batch of 4 samples attached to each other for sandblasting inside the chamber	29
Figure 3-8 Brush plating setup.....	30
Figure 3-9 Batch of samples plated with Zn-Ni.....	31
Figure 3-10 The XRF gun used to measure the coating thickness and Ni content.....	32
Figure 3-11 A schematic representation of a batch of samples attached to each other and placed in the sustained load test setup.....	33
Figure 3-12 Dummy samples used to replace fractured samples in SLT	33
Figure 4-1 Image of the Zn-Ni coating showing the two spots on the coating marked for elemental analysis	40
Figure 4-2 Evolution of coating morphology showing samples plated at a) 0.66 A/cm ² b) 2.0 A/cm ² c)3.3 A/cm ² d)5.3 A/cm ²	42
Figure 4-3 Coating morphology of a sample plated with standard plating parameters	43
Figure 4-4 Cross sectional image of a sample where through thickness micro-cracks in the coating are visible	43
Figure 4-5 SEM micrograph at the notch of a sample after sandblasting showing 3 alumina residue particles marked for EDS and elemental analysis	44
Figure 4-6 EDS analysis of particle 1 in figure 4-5	45
Figure 4-7 EDS analysis of particle 2 in figure 4-5	45
Figure 4-8 EDS analysis of particle 3 in figure 4-5	46
Figure 4-9 SEM image of the notch and surrounding areas of a sandblasted samples showing the visible residual alumina at low magnification	46
Figure 4-10 SEM image of the notch of a sandblasted sample plated with standard plating parameters after the end of the SLT showing a) the existence of cracks on the notch b) a higher magnification image to better show the presence of deep cracks.....	47
Figure 4-11 SEM image of the cracks in figure 4-10b demonstrating their depth	48
Figure 4-12 SEM image of the notch of the sample in Figure 4-10 after its coating was stripped showing a) the notch b) a higher magnification image of the notch to better show the cracks....	48
Figure 4-13 image of the notch of a sample without sandblasting and plated with standard plating parameters after the end of the SLT showing a) the notch b) a higher magnification image of the notch to better demonstrate the absence of cracks.....	49

Figure 4-14 SEM image of the surface of the first fractured sample from Test 1 showing a) fracture initiation region on the edge of the surface b) intergranular fracture at fracture initiation region c) dimples and ductile features becoming more dominant away from the fracture initiation region d) ductile fracture features at the centre of the fracture surface 50

Figure 4-15 SEM images of the surface of the second fractured sample from Test 1 showing a) fracture initiation region on the edge of the surface b) intergranular fracture at fracture initiation region accompanied by dimples and voids c) ductile features away from the fracture initiation region 51

Figure 4-16 Fracture surface of the first fractured sample from Test 6 showing a) fracture initiation region on the edge of the surface b) intergranular features at fracture initiation region c) ductile fracture surface away from the fracture initiation region 52

Figure 4-17 Fracture surface of the second fractured sample of Test 6 showing a) the fracture initiation region and b) the intergranular fracture alongside ductile dimples at the fracture initiation region..... 52

Figure 4-18 Fracture surface of the first fractured sample of Test 7 showing a) the fracture initiation region and b) the intergranular fracture alongside ductile dimples at the fracture initiation region..... 53

Figure 4-19 Fracture surface of the second fractured sample from Test 7 showing a) the fracture initiation region and b) the intergranular fracture alongside ductile dimples at the fracture initiation region..... 53

List of Tables

Table 1-1 Steel alloys used in airframes [15]	5
Table 2-1 The diffusion coefficient and permeation flux of hydrogen for Zn-Ni and Cd coatings with and without cracks [71].....	17
Table 3-1 Chemical composition of the investigated SAE 4340 steel.....	23
Table 3-2 Mechanical properties of SAE 4340 after heat treatment	24
Table 3-3 The industrial brush plating parameters	31
Table 4-1 SLT results for 4 experiments with different baking conditions	36
Table 4-2 SLT results of the samples plated at different constant plating current densities	37
Table 4-3 SLT results of the samples plated up to 175, 150, 125 and 60 A.s	38
Table 4-4 SLT results of the sample plated without sandblasting	38
Table 4-5- Elemental analysis of the two spots marked in figure 4-1	41
Table 4-6 Change in platelet size with variation in plating current density	42
Table 4-7 Elemental analysis of the three points marked as 1, 2 and 3 in figure 4-5	46

Chapter 1 : Introduction

Hydrogen Embrittlement (HE) has always been a serious problem notably in the aerospace industry where sensitivity is even higher. HE could degrade the mechanical properties of a metal and result in its premature failure in service. In this chapter, the fundamental theoretical concepts of HE and the challenges posed by HE in the aerospace industry will be discussed.

1-1 Fundamental concepts of hydrogen embrittlement

Hydrogen Embrittlement (HE) is a phenomenon in which the mechanical properties of metals deteriorate as a result of exposure to hydrogen. The first ever observation of the effect of HE was reported by Johnson in 1871 [1] when he discovered that the toughness of iron significantly deteriorates when immersed in acid and this effect is reversed overtime. This was attributed to hydrogen and not the acid given that the deterioration of mechanical properties only occurred in acids that produced hydrogen [1]. In 1926, Pfeil [2] discovered that the presence of hydrogen could cause a significant loss of ductility at room temperature under normal tensile loading conditions.

To understand the phenomenon of HE in metals, it is important to observe Hydrogen-Metal interactions and understand how hydrogen could find its way into the metal structure. In a service environment where metal comes in contact with a gas, three processes occur [3]:

- 1- The gas could condense on the surface of the metal and form a one or two molecule thick layer. This is called adsorption
- 2- The gas could then dissolve into the metal which is called absorption (or occlusion)
- 3- The absorbed gas could diffuse throughout the metal.

The adsorbed gas on the metal surface should dissociate into atomic form to diffuse into the metal [3]. Hydrogen adsorbs on the metal surface as H₂ molecules and then dissociates into atoms before diffusing into the metal. In such circumstances, the solubility of hydrogen in metals depends mostly on the temperature and the gas pressure [4-6].

In addition to gaseous conditions, hydrogen uptake could also occur during an electro-chemical process. The relevant reduction reactions resulting in the reduction and adsorption of hydrogen in these circumstances are as follows [7]:





These adsorbed hydrogen atoms either diffuse into the metal or may recombine to form gaseous molecular hydrogen as [7]:



1-2 Hydrogen in Metal Structure

1-2-1 Absorption into Metal Structure

After absorption into the structure of the metal, hydrogen tends to find itself in the interstitial sites in the lattice structure. In the case of Face-Centered Cubic (FCC), Hexagonal Close Packed (HCP) and Body-Centered Cubic (BCC) structures, hydrogen is likely to occupy the octahedral and tetrahedral interstitial sites [8]. Figure 1-1 demonstrates the octahedral (O) and tetrahedral (T) sites for these lattice structures. Octahedral sites are preferred by hydrogen atoms at temperatures beyond 100°C [9].

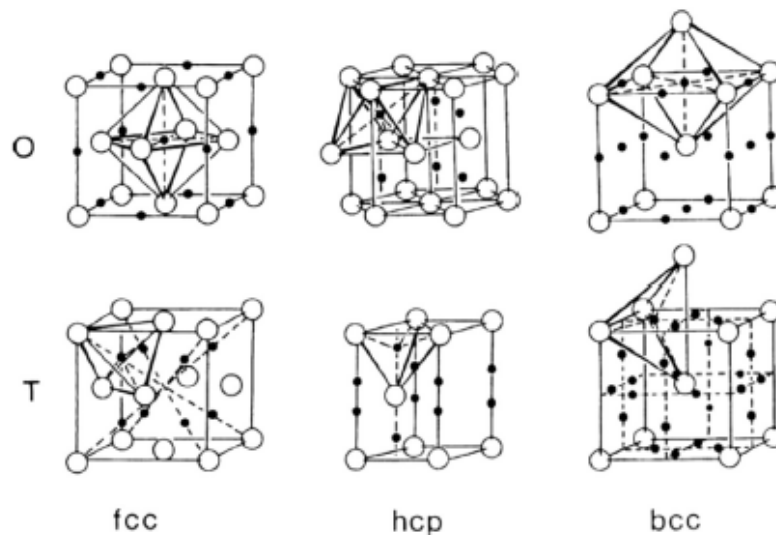


Figure 1-1 Interstitial sites (octahedral (O) sites and tetrahedral (T) sites) in FCC, HCP and BCC lattices [8]

1-2-2 Hydrogen Traps

As mentioned, small hydrogen atoms can easily diffuse into the metal structure and occupy interstitial sites [8-10] where they could be trapped by the microstructural defects of the host metal including dislocations, voids, grain boundaries, impurities and interfaces [10]. These traps are classified as irreversible and reversible traps [10]:

- 1) In irreversible traps, the activation energy for hydrogen to escape is high; therefore, the trapped hydrogen can no longer diffuse. Examples of such traps include incoherent precipitates and high angle grain boundaries.
- 2) In the case of reversible traps, due to lower activation energy, it will be easier for hydrogen to be released from the trap and thus it can diffuse within the structure. Examples of such traps are coherent precipitates, dislocations, low angle grain boundaries and twin boundaries.

Figure 1-2 illustrates various hydrogen traps in the microstructure [11].

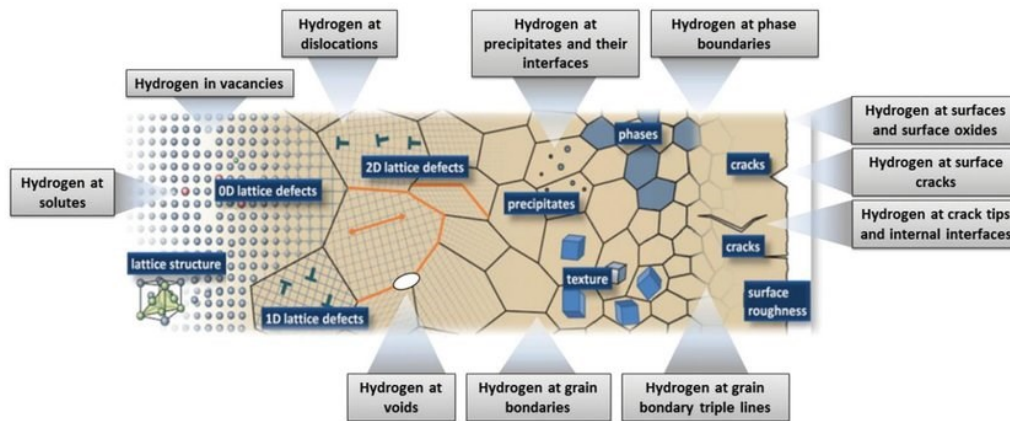


Figure 1-2 Schematic illustration of hydrogen traps sites [11]

For crack initiation, a critical concentration of hydrogen is necessary in hydrogen traps [12]. This critical concentration depends on the shape, size and location of that trap within the lattice structure [12]. For example, lower hydrogen concentration is required to initiate crack from elongated MnS inclusions than from round MnS inclusions and it is reported to be more pronounced in segregated bainite-martensite zones than in ferrite-pearlite structures [13]. The capability of a material to reversibly trap hydrogen is also an important factor in determining its susceptibility to HE [14].

1-3 Problem statement

Having explained the history and fundamentals, it is important to discuss its relevance in the context of this research and clarify how HE might be an issue in Zn-Ni electro-plated components.

In aircraft production, by far the most widely used material is aluminum and the use of light weight alloys as well as composite materials is on the rise [15,16]. However, in many critical components of the aircraft such as landing gear, steel is the preferred material due to its good stiffness, high tensile strength and wear resistance [15,16]. Table 1-1 summarizes the steel alloys used in airframes:

Table 1-1 Steel alloys used in airframes [15]

Alloy	Examples	Typical Usage
Carbon and low alloy steels	T1: Fe, 0.15C, 0.92Mn, 0.88Ni, 0.5Cr, 0.46Mo, 0.32Cu, 0.26Si 4130: Fe, 0.3C, 0.95Cr, 0.2Mo	Used where the required strength is less than 700 MPa
High strength steels	4340: Fe, 0.4C, 1.8Ni, 0.8Cr, 0.25Mo 8630: Fe, 0.3C, 0.55Ni, 0.5Cr, 0.25Mo	Landing gear components, pinions, connecting rods, bolts.
Austenitic stainless steels	316: Fe, 18Cr, 13Ni, + Mo 347: Fe, 18Cr, 12Ni, + Nb 310: Fe, 25Cr, 20Ni	Mostly used in engines and low volume parts in the airframe where corrosion resistance is required
Martensitic stainless steels	403: Fe, 12Cr, low carbon 440: Fe, 17Cr, 0.5Mo, high carbon	High strength fasteners and forgings, cold drawn thin section parts, aircraft pressure vessels
Age hardened steels	AM362: Fe, 15Cr, 7Ni, Ti	Turbine discs, exhaust components. Limited use in airframe

High strength steels such as 4340 and 8630 have superior strength and can be used in places where the required yield strength is beyond 1400 MPa with the most common being in landing gears [15]. However, corrosion resistance of these alloys is low and thus require protection [15]. This is done using a variety of electro-plating procedures the most common of which are Cr, Cd and the emerging Zn-Ni electro-plating processes. Cr and Cd electro-plating provides good wear and

corrosion resistance properties [15]. However, both of these processes produce dangerous carcinogenic by-products [17-19] and Zn-Ni is gaining traction as an environmentally-friendly alternative to these two processes. But regardless of their properties or toxicity, the issue that will inevitably arise is the exposure of the landing gear to hydrogen and subsequent HE as a result of the electro-plating procedure. This problem is pronounced in the case of landing gears since the high strength steels used to manufacture them are very susceptible to HE [15,20]. Thus, research such as the work presented in this thesis is of paramount importance to identify and mitigate HE in industrial processes where high strength steel is involved.

1-4 Thesis layout

This thesis consists of 5 chapters. The introductory chapter served to introduce the fundamentals of HE and clarify how it can become an issue during electro-plating. Chapter 2 will be dedicated to reviewing the literature pertinent to the subject of this thesis which includes HE evaluation and characterization, HE mechanisms, Zn-Ni electro-plating, HE in Zn-Ni electro-plating and finally brush plating. Chapter 3 will elaborate the methodology, sample preparation process, HE evaluation instruments and plating process parameters used in this research. In chapter 4, the results derived from the HE evaluation experiments as well as the microscopic observations of the samples will be discussed. Finally, chapter 5 will summarize the conclusions and contributions of this work as well as provide recommendations for future research.

Chapter 2 : Literature review

This chapter will begin by discussing the literature relevant to HE evaluation methods and mechanisms. Subsequently, the relevant literature concerning Zn-Ni electro-plating and its HE tendencies will be discussed. Finally, the pertinent literature regarding brush plating will be reviewed.

2-1 Hydrogen embrittlement evaluation and characterization methods

Degradation of mechanical properties under the influence of hydrogen is well documented and it could affect a wide range of properties such as tensile strength, fracture toughness, hardness and elongation to fracture [21-24]. However, evaluation of mechanical properties is the oldest approach to HE analysis and a more contemporary approach is to accompany such tests with molecular dynamics (MD) simulations or microscopic observations [25]. MD simulations focused on HE do not fall within the scope of this thesis and mechanical testing accompanied by fractography is more pertinent. The ASTM F519 [26] standard is one of the most well-known HE evaluation standards that provides a good basis for HE evaluation of electro-plated parts using standardized mechanical tests. This standard is used in the present research and its test methods will be explained in more detail in chapter 3. There are other research endeavors that have used this standard as the basis of their experiments as well [27-29].

The subsequent fracture surface micrography can be done using optical microscopy (OM), scanning electron microscopy (SEM) or transmission electron microscopy (TEM) [30]. Features such as the location of crack initiation, possible secondary cracking, fracture along phase boundaries or particular phases in the microstructure, phase transformation around crack tips etc. [30] can also be revealed using these tools. Fractography had an instrumental role in the discovery and development of HE mechanisms such as pressure expansion theory [31] and hydrogen enhanced localized plasticity (HELP) [32]. However, among these tools, it is much easier to use SEM for fracture surface observations rather than TEM since less preparation is required for SEM samples and the features that can be seen with TEM are also observable using SEM [29,33,34]. Among these features is intergranular fracture that is easily identifiable with SEM and its presence on the fracture surface is known to indicate HE [26,35].

2-2 Mechanisms of hydrogen embrittlement

The effects of HE on the mechanical properties of metals have been the subject of research for a long time and multiple mechanisms have been proposed to explain this phenomenon. In this section, the most widely known HE mechanisms will be reviewed. There is considerable disagreement among researchers regarding the characteristics of these mechanisms and their role in a metal exposed to hydrogen and despite extensive research, they are not yet fully understood [35,36,37]. These proposed mechanisms include but are not limited to:

- 1- Hydrogen Enhanced De-Cohesion (HEDE) [2,30,38,39]
- 2- Hydrogen Enhanced Localized Plasticity (HELP) [32,40,41]
- 3- Hydride formation and cleavage [42,43]
- 4- Adsorption Induced Dislocation Emission (AIDE) [36,44]
- 5- Hydrogen Enhanced Strain Induced Vacancy (HESIV) [6,45]

However, among these mechanisms, the most widely investigated are HEDE and HELP.

2-2-1 Hydrogen Enhanced De-Cohesion (HEDE)

HEDE was initially proposed by Pfeil in 1926 [2] when it was concluded that hydrogen reduces the cohesion of the structure across cubic cleavage planes as well as grain boundaries. Oriani [39] later developed this theory stating that interatomic bonds are weakened with the presence of hydrogen due to charge transfer leading to the tensile separation of the atoms [39]. However, obtaining direct evidence of HEDE is difficult since it is impossible to observe events at atomic scale around crack tips [46]. But the weakening of bonds is supported by the fact that surface atoms evaporate easier during field ion microscopy when hydrogen is used as an imaging gas [47]. Figure 2-1 illustrates the ways in which hydrogen can weaken interatomic bonds. It should be noted that for HEDE mechanism to be activated, the local hydrogen concentration should reach beyond a critical threshold level [48]. Intergranular fracture is a manifestation of this mechanism [37,48]

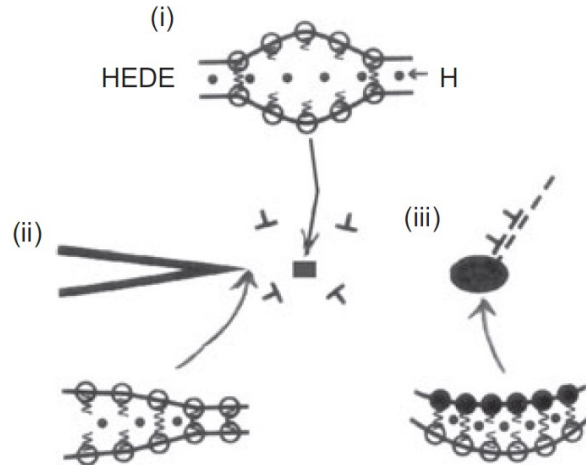


Figure 2-1 schematic illustration of HEDE mechanism showing the separation of atoms due to interatomic bonds by (i) presence of hydrogen in the lattice structure (ii) hydrogen being dissolved and (iii) presence of hydrogen at particle-matrix interfaces [48]

2-2-2 Hydrogen enhanced localized plasticity

This mechanism was first proposed by Beachem in 1972 [32] based on fractographic observations. Alongside the HEDE mechanism, HELP is also widely discussed in research surrounding the mechanisms of HE and carries equal importance as HEDE. Beachem [32] stipulated that fracture occurred due to hydrogen facilitating dislocation movement given that the fracture surface had ductile features. Hydrogen tends to concentrate near crack tips thus leading to localized deformation near the crack tip and facilitates dislocation movement [32,48]. Therefore, subcritical crack growth occurs due to localized micro-void coalescence and creates ductile features such as dimples on the fracture surface [32,48]. A schematic illustration of this mechanism is shown in Figure 2-2 [48].

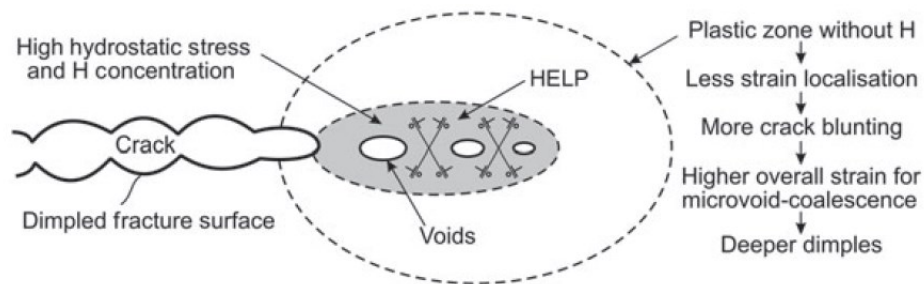


Figure 2-2 Schematic illustration of HELP mechanism demonstrating the coalescence of micro-voids and plasticity being localized in areas of high hydrogen concentration [48]

Direct evidence of hydrogen facilitating dislocation movement has been proposed in the literature as well. An example of this phenomenon is reported by Shih et al. [49] as they concluded that the

presence of hydrogen accelerated dislocation motion and caused new dislocations to appear. The removal of hydrogen gas caused the dislocations to stop moving and its reintroduction caused dislocation movement to accelerate.

2-2-3 Interaction and synergy of various hydrogen embrittlement mechanisms

As mentioned earlier, the interactions between hydrogen and the metal are not yet fully understood and the mechanisms of HE are not yet completely clear. The factors that influence these interactions and mechanisms include: 1- the source of hydrogen (gaseous or electro-chemical) 2- the global and local content of hydrogen in the material 3- hydrogen concentration gradient 4- the local trapping process of hydrogen or its distribution 5- microstructure [36]. Depending on these factors, the effects of the presence of hydrogen could differ and at times show opposite and contradictory characteristics [37,50-52]. It is also important to note that the effect of hydrogen on the plasticity of material is not just limited to the HELP mechanism and could manifest itself in other mechanisms discussed in the literature such as hydrogen-enhanced strain-induced vacancy (HESIV) [6,45] and adsorption induced dislocation emission (AIDE) [37,44,48]. The HESIV mechanism is based on the notion that the presence of hydrogen increases the formation and clustering of strain induced vacancies while the AIDE mechanism stipulates that the absorption of hydrogen facilitates both the nucleation and the subsequent movement of the dislocation away from the crack tip leading to the formation of comparatively shallow dimples on the fracture surface. Under sustained load, the AIDE mechanism will result in the formation of micro-voids and nano-voids that contribute to crack growth [48]. These mechanisms could work in tandem to embrittle a metal. An example of the synergy between HELP and HEDE mechanisms was reported by Novak et al. [53]. In their work, notched samples manufactured from heat treated 4340 high strength steel were charged using hydrogen gas and subsequently subjected to a four-point bending test. It was revealed that hydrogen charging will cause fracture to initiate ahead of the notch root at carbide/matrix interface and exhibit intergranular fracture features as shown in Figure 2-3.b. It was stipulated that the brittle intergranular fracture occurs as a result of a pile-up and impingement of dislocations at the interface of grain-boundary carbide and matrix due to their facilitated movement resulting from the HELP mechanism. These dislocations transported hydrogen along with them to the carbide/matrix interface, increasing hydrogen concentration at the carbide/matrix interface thus activating the HEDE mechanism which manifests itself in the form of intergranular fracture.

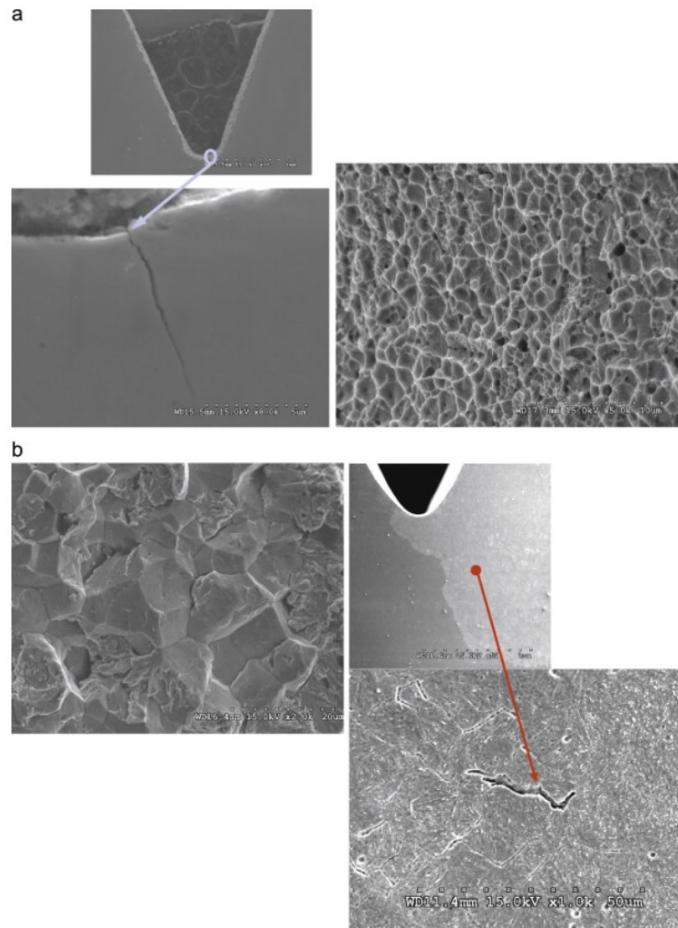


Figure 2-3 a) Fracture surface of the uncharged sample showing ductile fracture initiating at the notch b) Fracture surface of the charged sample showing intergranular fracture initiating ahead of the notch [53]

Another example of the co-existence of multiple HE mechanisms was reported by Matsumoto et al. [54] via MD simulations. In their research, they simulated the tensile deformation of an iron nano-rod under the influence of hydrogen and compared it to an identical simulation without hydrogen influence revealing that in the presence of hydrogen, fracture occurs quickly along grain boundaries and is accompanied by significant dislocation activity and the formation of vacancies. This is a clear manifestation of the HEDE, HELP and HESIV mechanisms working in tandem. Nano-indentation simulations carried out in the same research by Matsumoto et al. [54] also demonstrated identical results. Similar MD simulations by Solanki et al. [55] confirmed the synergy of HELP and AIDE mechanisms as well.

2-5 Zn-Ni electro-plating

As discussed in chapter 1, Cd is used as a protective coating on aircraft components such as landing gears. However, Cd and its compounds are extremely toxic [56]. The poisonous nature of its salts will make it difficult to dispose of them after electro-plating and the permissible levels of Cd that can be discharged into the environment are extremely low and subject to severe restrictions in many countries [56]. Moreover, the use of cyanide baths for Cd electroplating further exacerbates the issue of toxicity in Cd electro-plating [56]. Therefore, Zn-Ni is gaining traction as an alternative to Cd [57-59]. Zn-Ni coatings are found to provide better corrosion resistance for steel than galvanized Cd coating as well as pure Zn coating [59,60]. The Ni content of the coating plays an important role in its corrosion protection properties. It is reported in the literature that a Ni content between 10-15% provides optimum resistance to corrosion which corresponds to γ Zn-Ni [61,62]. The Zn-Ni phase diagram in Figure 2-4 shows the composition range of the γ phase.

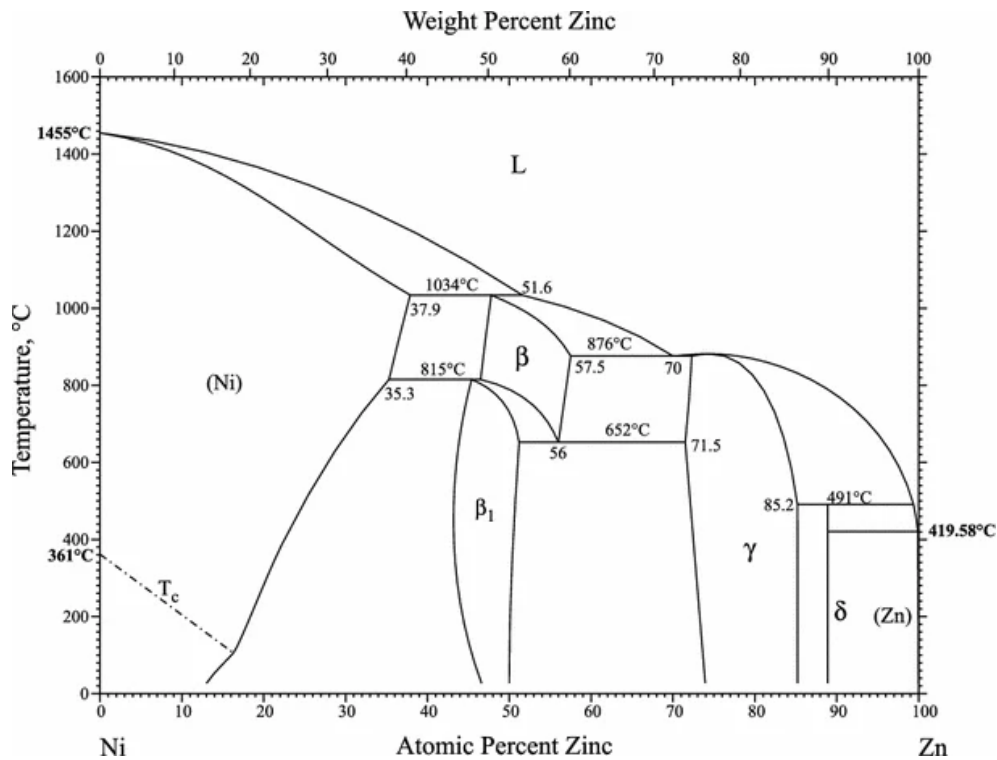


Figure 2-4 Zn-Ni phase diagram [63]

Different morphologies have been reported for Zn-Ni coatings depending on the pH and composition of the plating bath. Felloni et al. [64] reported a pyramid crystallite structure for Zn-

Ni coatings deposited from an acidic chloride bath. Figures 2-5 and 2-6 show the SEM micrographs of the morphologies of Zn-8.5%Ni and Zn-14%Ni coatings demonstrating their pyramid structure.

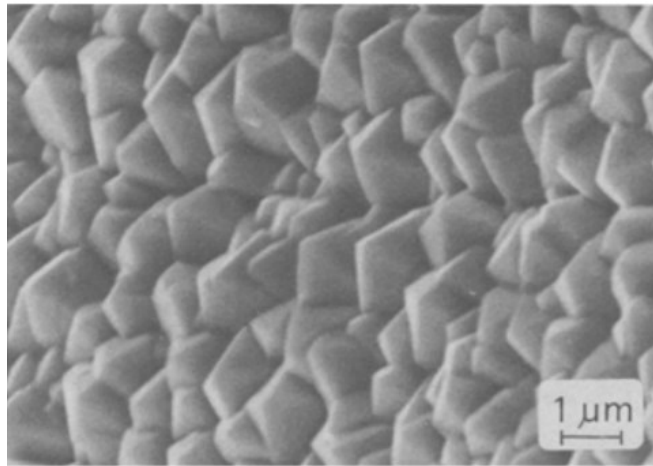


Figure 2-5 Electro-deposited Zn-Ni coating with 8.5% Ni at a current density of 5mA/cm² [64]

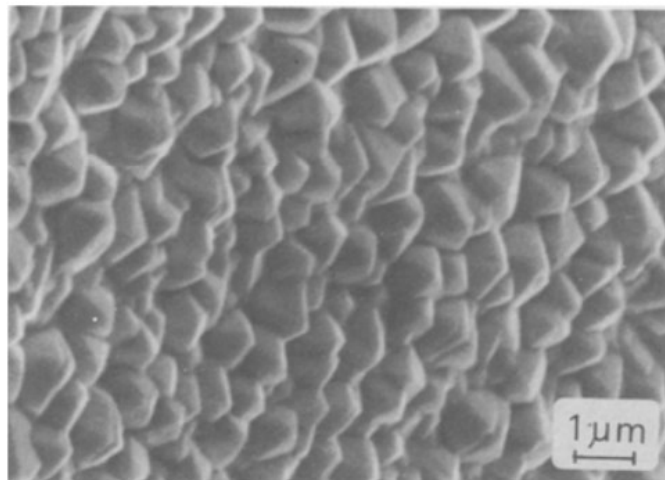


Figure 2-6 Electro-deposited Zn-Ni coating with 14% Ni at a current density of 5mA/cm² [64]

On the other hand, Rajagopalan et al. [65] reported a platelet-like morphology for Zn-Ni coatings deposited from an alkaline solution. Figure 2-7 shows the morphology of the deposited coatings plated at 30 mA/cm² and 48 mA/cm². This was also confirmed by Conde et al. [59] as they obtained a similar morphology from their alkaline bath as shown in Figure 2-8. Alkaline baths are preferred in applications where the substrate material is more susceptible to HE such as high strength steel as they are reported to cause less HE compared to acidic baths [59]. The solution used in the present research is alkaline as well which is preferred for electro-plating embrittlement susceptible parts such as landing gears.

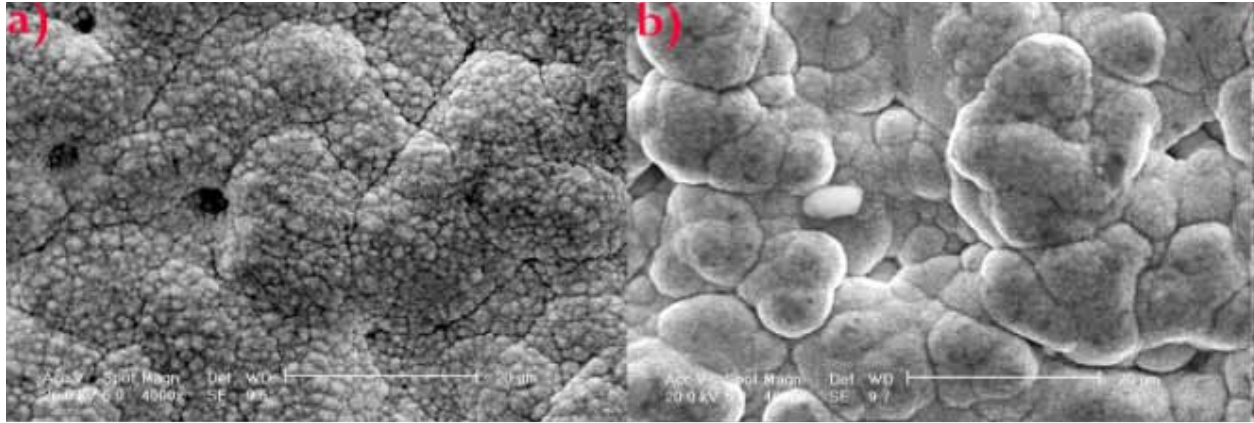


Figure 2-7 Zn-Ni coating deposited at a) 48 mA/cm² and b) 30 mA/cm² [65]

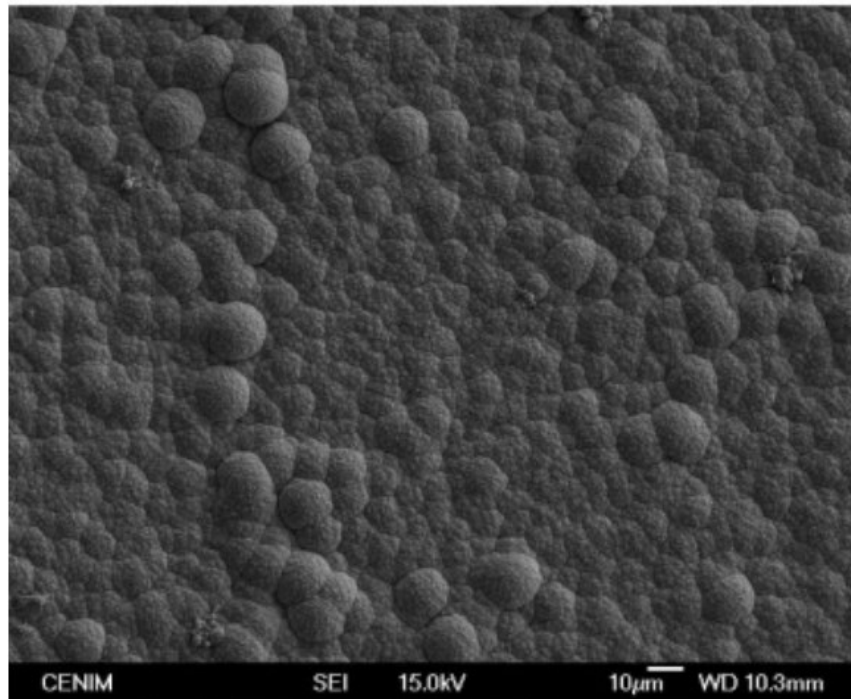


Figure 2-8 SEM micrograph of Zn-Ni coating deposited at 15 mA/cm² with 14% Ni [59]

2-4 Hydrogen embrittlement in Zn-Ni and Cd electro-plated coatings

As mentioned in the introduction, Cd and Zn-Ni coatings are applied on landing gears in the aerospace industry to protect them against corrosion [15]. Moreover, they can also act as strong diffusion barriers against hydrogen diffusion [66]. Cd accelerates the recombination of hydrogen atoms to prevent their diffusion into the substrate while Zn-Ni coatings considerably impede hydrogen diffusion thanks to the formation of an initial Ni-rich layer [66,67]. However, the electroplating processes used to deposit these coatings could themselves expose the substrate to hydrogen

that can diffuse into it [66,67]. As a result, it is common practice in industry to carry out a HE relief bake after electro-plating. This is done by subjecting the electro-plated workpiece to baking within 4 h after electro-plating at a temperature of 190°C for a duration of 24 h to allow hydrogen to diffuse out of the material [68].

It is also important to note that the diffusion of hydrogen through these coatings is largely dependent on the existence of micro-cracks, discontinuities, pores and defects in the coating and such features can affect HE susceptibility both during the electro-plating process and in-service environments [69,70]. Rajagopalan et al. [71] concluded that micro-cracks, coating discontinuities and porosity facilitate the diffusion of hydrogen in a coating that will otherwise significantly impede this diffusion. Figure 2-9 shows that Cd and Zn-Ni coatings with microcracks and discontinuities recorded a much higher rate of hydrogen permeation when studied using Devanathan-Stachurski double cell. The diffusion coefficient and the permeation flux were also quantified as shown in Table 2-1. Diffusion coefficient is an indication of the capacity of a substance to diffuse across a unit area in a timespan of 1s as a result of concentration gradient of that substance while the permeation flux is the amount of substance that diffuses across a unit of area in 1s [72,73].

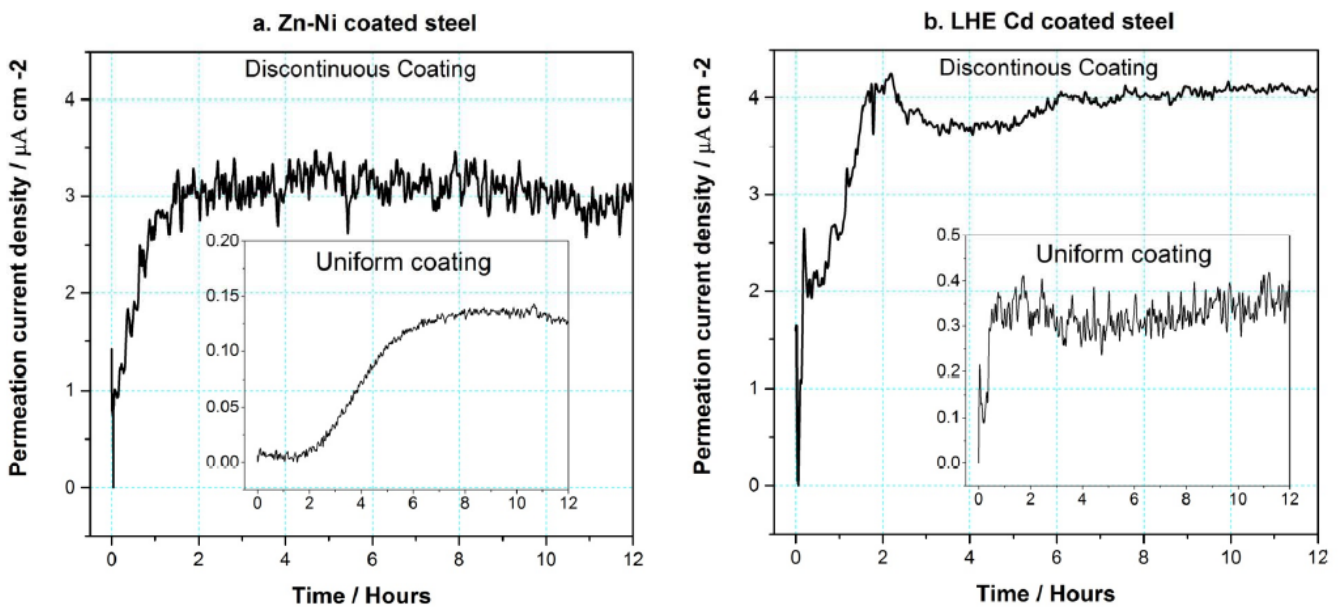


Figure 2-9 Permeation current density plotted against time for both Zn-Ni and Cd coatings [71]

Table 2-1 The diffusion coefficient and permeation flux of hydrogen for Zn-Ni and Cd coatings with and without cracks [71]

Material	Diffusion Coefficient $D \times 10^{-8}$ ($\text{cm}^{-2} \text{s}^{-1}$)	Permeation flux $J_{ss} \times 10^{-11}$ ($\text{mol s}^{-1} \text{cm}^{-2}$)
Zn-Ni	0.391	0.087
Zn-Ni with microcracks and discontinuities	5.778	3.177
Cd	4.543	0.378
Cd with micro-cracks and discontinuities	25.135	4.183

Plating parameters such as current density and bath pH affect the permeability of the coating and the HE susceptibility of the electro-plating process as well. Carr and Robinson [74] reported that Zn-Ni plating in a bath with a pH of 2 leads to significantly less hydrogen uptake compared to a bath with a pH of 5 despite hydrogen concentration being higher at a lower pH. This is explained by the formation of a thin pure Ni layer at the early stages of the deposition at lower pH which acts as a strong diffusion barrier for hydrogen. The influence of current density was investigated by Rajagopalan et al. [65] showing that coatings plated at a higher current density allowed less hydrogen permeation as demonstrated by the permeation current transients in Figure 2-10. Moreover, Ghaziof et al. [75] reported that increase in plating current density results in higher Ni deposition at the expense of hydrogen thus leading to a higher Ni content in the coating and less hydrogen diffusion.

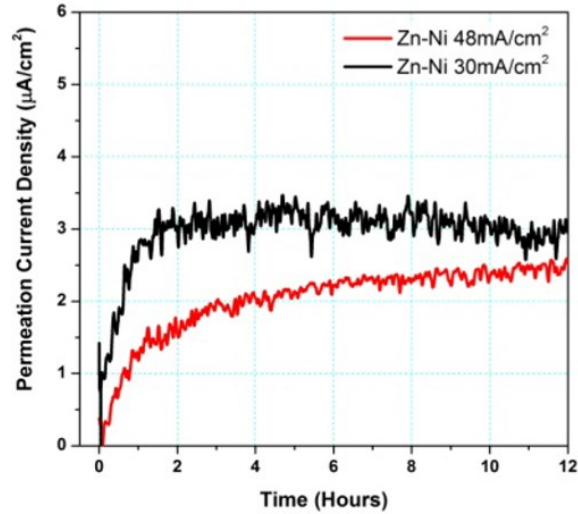


Figure 2-10 Hydrogen permeation current transient for the Zn-Ni coatings plated at 30A/cm² and 48A/cm² [65]

Nevertheless, an excessively dense and impermeable coating could be undesirable during baking. As reported by Bellemare et al. [76], a highly dense coating will considerably reduce the efficiency of the embrittlement relief to the point that the baking temperature must be increased for adequate embrittlement relief. The influence of baking and its temperature will be discussed further in chapter 4 of this thesis as the electro-plating process in this research had a very efficient embrittlement relief response.

Zn-Ni coatings have shown desirable properties regarding HE. Hillier et al. [77] reported that electro-plating of Zn-10%Ni coatings caused significantly less embrittlement than Zn-Co coatings and slightly less embrittlement than Cd coatings. It was also shown that even with baking, the Zn-Co electro-plating process caused more embrittlement than Zn-Ni without baking. The low HE susceptibility of the Zn-Ni coating was attributed to the formation of the Ni-rich layer at the coating/substrate interface preventing hydrogen diffusion during electro-plating. Conde et al. [59] reported that alkaline Zn-Ni electro-plating, if done at optimum plating parameters to produce a dense coating with high Ni content, incorporates less hydrogen into the substrate than Cd electro-plating would even after baking. This is also a major point of discussion in chapter 4 as opposite results were obtained for the Zn-Ni brush plating process. Rajagopalan et al. [65] also reported that Zn-Ni electro-plating produces less hydrogen compared to Cd and pure Zn and has a very efficient baking response owing to the existence of defects and micro-cracks in the coating structure.

2-5 Brush plating

Zn-Ni electro-plating and its properties were discussed in the previous two sections. However, the focus of the present research is on Zn-Ni brush plating. Brush plating is a versatile plating process that can be used to carry out in-situ plating or repair damaged coatings [78]. The coating is deposited using a brush tool that puts the electro-plating solution in contact with the work piece under direct current (DC) via a portable rectifier [78]. The electro-plating solution is replenished either by intermittently dipping the brush in the solution or by using a manual dispenser to imbibe the brush while it is in contact with the work piece [78]. There are also disadvantages to the brush plating process such as its labor-intensive nature which makes it prone to human errors as well as the expensive proprietary solutions [78]. Nevertheless, the versatility of the process will make it a suitable choice for depositing a wide range of coatings such as Cd, Cu, Ni alloys etc. and it has gained widespread industry acceptance with well over 100 industry specifications written for various industries such as oil, aerospace, automotive, power generation etc. [79]. Automated brush plating procedures have also been developed to eliminate the human errors of manual brush plating and have been reported to create a much more uniform and dense coating with higher hardness [80,81]. Figure 2-11 demonstrates the difference between a manually plated Ni/nano- Al_2O_3 composite coating and an automatically plated one. Gaps and pinholes can visibly be seen in the manually deposited coating. This is to be expected since the operator in the manual process cannot maintain the same contact pressure and contact area between the brush and the workpiece at all times. The brush plating process investigated in this research is manual as well and demonstrates similar characteristics.

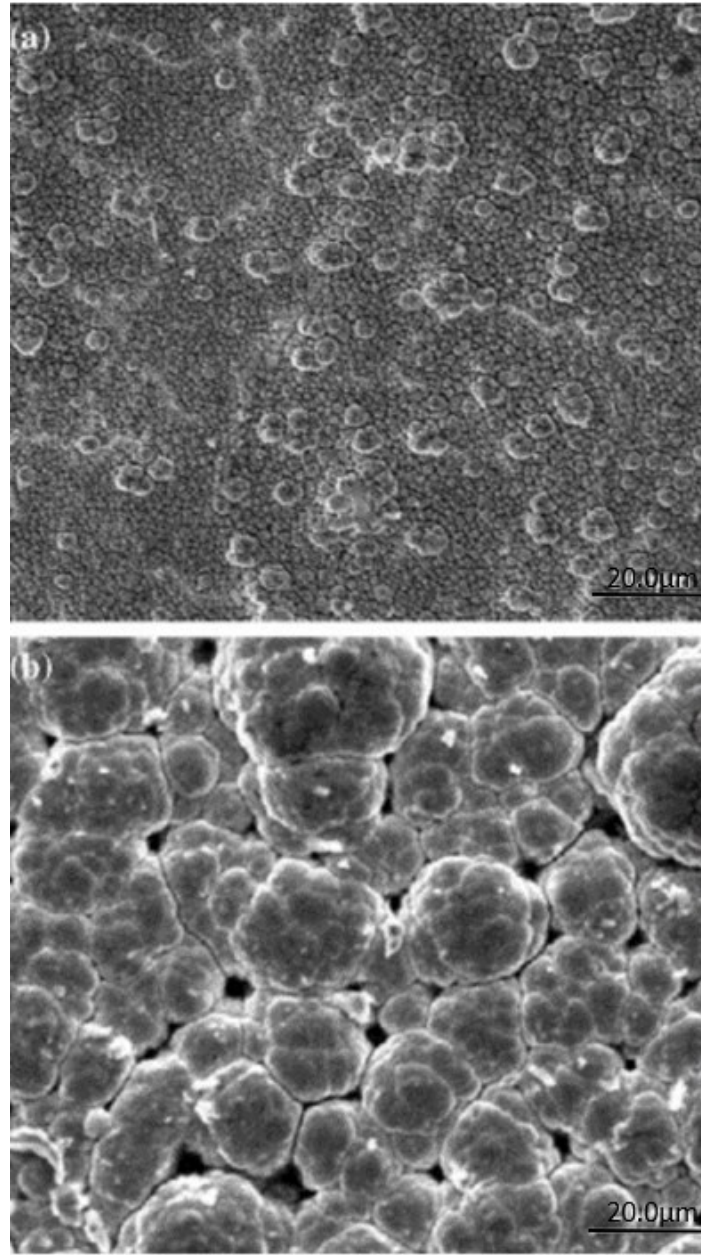


Figure 2-11 SEM surface morphology of Ni/nano- Al_2O_3 composite coating: (a) automatically plated and (b) manually plated [81]

Brush plating parameters are instrumental in determining the properties of the deposited coating. Parameters such as current density, contact pressure between the brush and the workpiece as well as the speed of the movement of the brush relative to the workpiece can affect coating morphology, hardness, elastic modulus and wear resistance [82]. Pinholes and gaps in the coating can be eliminated if the relative speed of the anode to the workpiece surpasses a threshold value whereas high contact pressure can create cracks in the coating [82]. HE susceptibility is also affected by

the plating parameters. Behera et al. [83] examined the HE of three Zn-Ni brush plated coatings deposited at constant voltages of 6, 10 and 12 V using an incremental step load (ISL) test. The Zn-Ni coating plated at 6 V passed the ISL test embrittlement threshold while those plated at 10 and 12 V did not. They also discovered that brush type plays a considerable role in HE severity as the sample plated at 12 V with a graphite brush failed the embrittlement test while those plated using a Ti brush passed. However, Cd brush plating was reported to be less embrittling and had a much lower hydrogen permeation rate than all the examined Zn-Ni samples plated at different conditions.

2-6 Research objectives

The work presented in this thesis is industrially driven and the research behind it was carried out in collaboration with Safran Landing Systems as the industrial partner. The focus of this research is Zn-Ni brush plating process since it is expected to replace Cd in the near future. The objectives can be summarized as follows:

- 1- Determining the important factors in HE of the Zn-Ni brush plating process using the ASTM F519 standard
- 2- Mitigate the embrittlement issues of the Zn-Ni brush plating process and provide insights to Safran Landing Systems by analyzing the process from sample preparation to baking to facilitate the implementation of the Zn-Ni process as a replacement for Cd.

Chapter 3 :

Experimental Procedure

In this chapter, the experimental procedure to evaluate the HE susceptibility of an electro-plating process will be explained. This includes the information regarding the material used, sample preparation, brush plating process and finally the SLT for HE evaluation.

3-1 Sample material

The tests to evaluate HE were conducted in accordance with ASTM F519 [26]. The sample preparation steps including manufacturing, heat treatment and validation of the mechanical properties of the samples were done by Green Specialties Ltd. as the certified supplier of the samples to Safran Landing Systems. The raw material used is air melted SAE 4340 steel as per AMS 6415 [84] whose composition is listed in Table 3-1 as provided by Green Specialties Ltd.

Table 3-1 Chemical composition of the investigated SAE 4340 steel.

Element	C	Mn	P	S	Si	Cu	Ni	Cr	Mo	Sn	Al	V	Co	W
Content (wt. %)	0.4	0.72	0.02	0.023	0.27	0.17	1.67	0.77	0.25	0.002	0.026	0.02	0.011	0.004

In order to achieve the high strength required by the standard, the material was austenitized in a vacuum furnace at a temperature of 829°C for 1 h then subsequently quenched in oil. Afterwards, it was double tempered at 232°C for 4 h each. The response to this heat treatment operation was evaluated via 4 tensile tests and 100 hardness measurements to ensure that mechanical properties are within the specified range. The average values of the evaluated mechanical properties are listed in Table 3-2. The aforementioned heat treatment procedure and the validation of the mechanical properties was done by Green Specialties Ltd. The resulting microstructure was also analyzed and shown in Figure 3-1. As expected, the heat treatment produced the desired martensitic microstructure.

Table 3-2 Mechanical properties of SAE 4340 after heat treatment

Mechanical Properties	Value
Hardness	52 HRC
Tensile Strength	1865 MPa
Yield Strength	1558 MPa
Elongation	13%
Reduction of Area	48%

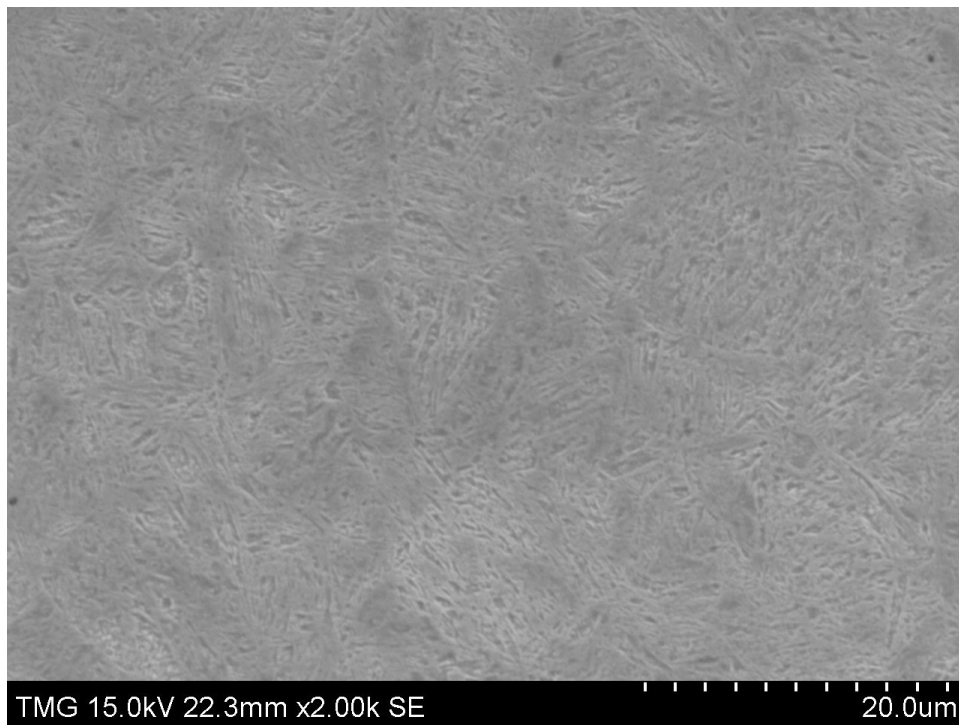


Figure 3-1 SEM image of the microstructure of the samples used in this research

3-2 Sample preparation

The notched bar samples shown in Figure 3-2 were used for HE evaluation testing. These samples correspond to the sample type 1a.1 of ASTM F519 [26]. The samples were machined from the heat-treated SAE 4340 steel and were subsequently subjected to a stress relief bake at $190\pm 14^{\circ}\text{C}$ as per AMS 2759/11 [85] for 4 h after machining. Figures 3-3 and 3-4 show images of an as-received sample and its notch respectively.

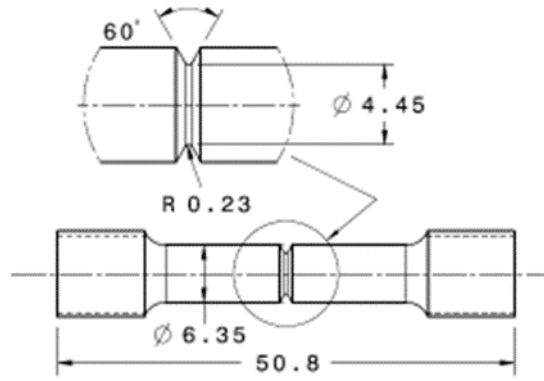


Figure 3-2 Layout of type 1a.1 sample (dimension are in mm) [26]

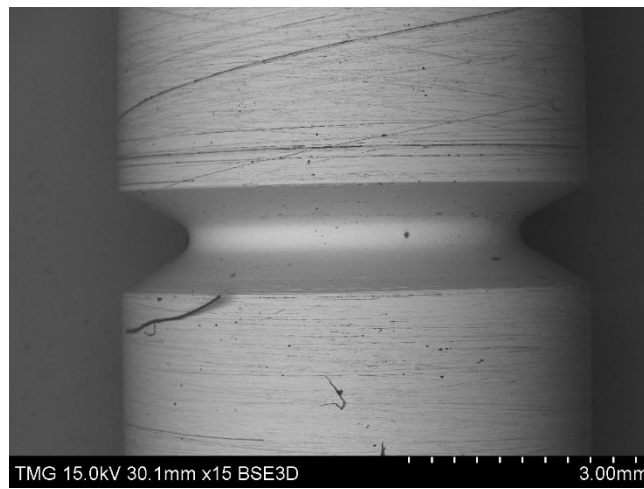


Figure 3-3 SEM image of an as-received test sample

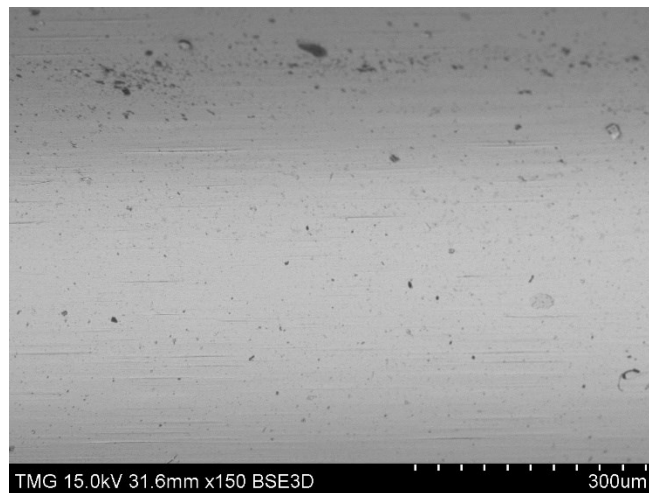


Figure 3-4 SEM image of the notch of an as-received test sample

3-3 Plating procedure

3-3-1 Introduction to brush plating

The plating process analyzed in this research is brush plating. A quick plating process that is used in aerospace industry to repair damaged coatings. The setup of this process is portable consisting of a rectifier, a brush (which is connected to the anode) and a plating solution instead of a bath. The part to be plated (substrate) is attached to the cathode, the coating on the substrate is deposited by pouring the plating solution on it and simultaneously rubbing the brush against the substrate. Figure 3-5 is an illustration of the brush plating setup.

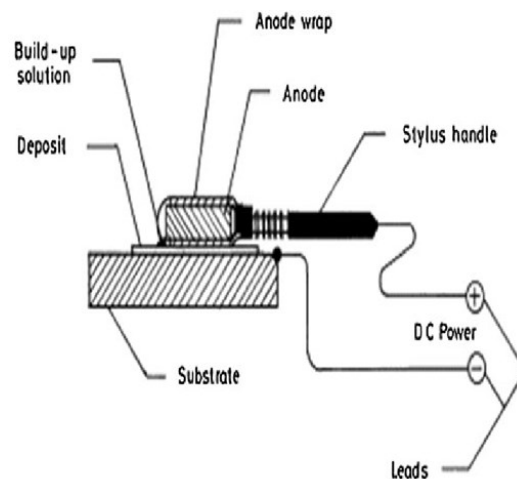


Figure 3-5 Schematic representation of the brush plating setup [86]

The anode and the cathode are connected to the rectifier shown in Figure 3-6. The plating parameters are displayed on different screens on the rectifier as marked on the image in Figure 3-6, these parameters include:

- 1- The plating voltage which is usually kept constant in the brush plating process.
- 2- The plating current usually varies during brush plating. However, it can be fixed at a constant value instead of plating voltage depending upon the user requirements.
- 3- The total electric charge, Q (in ampere-seconds (A.s) or ampere-hours (A.h)), passed through the system during the plating process which is displayed on the ampere-hour meter.



Figure 3-6 Rectifier used for brush plating

The total electric charge is used for calculating coating buildup. The thickness of the coating to be deposited on the substrate can be determined theoretically using Faraday's first law of electrolysis which stipulates that the mass of the electroplated metal during plating is directly proportional to the electric charge that has passed through the system and is formulated by equation 3.1 [87,88]

$$m_{th} = \left(\frac{M}{nF} \right) Q \quad \text{Eq. 3-1}$$

where Q is the total electric charge that has passed through the system (in Coulombs or A.s), m_{th} is the theoretical mass of the deposited metal, M is the molar mass of the metal, n is the number of electrons and F is Faraday's constant. Also, the mass of the deposited metal, m_{th} , can be calculated as [87]:

$$m_{th} = \rho A t_{th} \quad \text{Eq. 3-2}$$

where ρ is the density of the deposited metal, A is the plating surface area and t_{th} is the theoretical thickness of the deposited coating. By substituting Equation 3-2 into Equation 3-1, the relation between the theoretical thickness of the deposited metal and the electric charge that has passed through from the anode to the cathode during plating process can be established as [82]:

$$t_{th} = \left(\frac{M}{\rho n F} \right) \frac{Q}{A} \quad \text{Eq. 3-3}$$

The term $\left(\frac{M}{\rho nF}\right)$ is called the electrochemical equivalent which is often denoted by Z and is unique for every solution. Therefore, if the surface area of the substrate to be plated is known, the total electric charge, Q , required to deposit a coating with a desired thickness can be theoretically calculated using Equation 3-3.

3-3-2 Pre-plating preparations and sandblasting

The industrial procedure of plating the test samples requires certain preparations beforehand. First, the samples are visually inspected to make sure that there are no signs of damage to the notch and the samples surface. Afterwards, they are sandblasted in order to create an appropriate surface roughness to ensure proper coating adhesion. In this research, all the experiments except for one were carried out using sandblasted samples. Sandblasting was performed using an automated setup to ensure its uniformity. Samples are attached to each other and placed in the sandblasting chamber as shown in Figure 3-7. Subsequently they are sandblasted by a robotic nozzle at a pressure of 25 psi (0.172 MPa). The robotic nozzle maintains a distance of 350 mm and is positioned at an angle of 70° from the samples. After sandblasting, the samples are scrubbed and observed using a low magnification optical microscope to reassure the integrity of the notch before conducting brush plating.

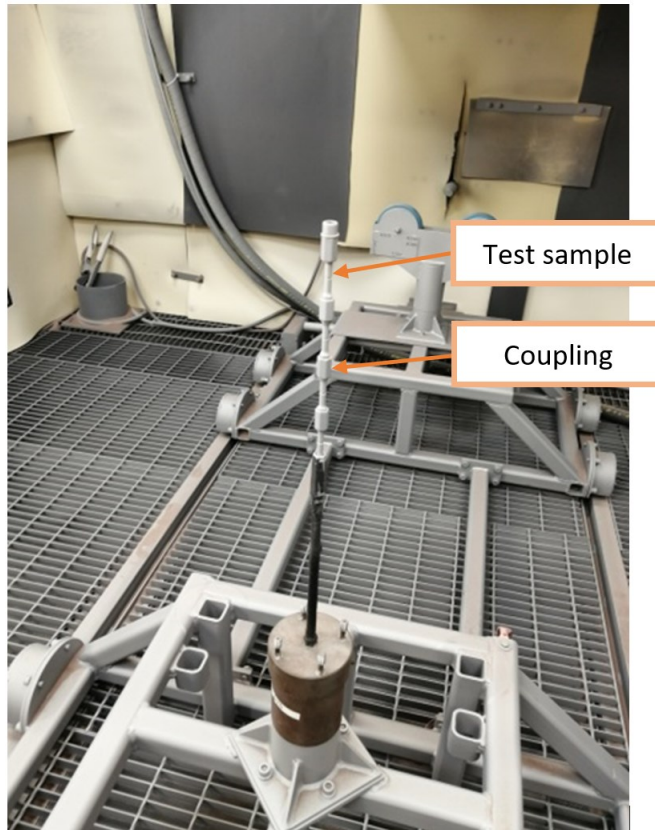


Figure 3-7 Batch of 4 samples attached to each other for sandblasting inside the chamber

3-3-3 Plating parameters

During plating, the samples are connected to the cathode of the rectifier and rotated at a constant rate of 60 rpm to ensure a uniform deposition of coating. The brush is attached to the anode and is manually kept in contact with the sample surface as the plating solution is poured onto it until the coating is built up to the desired thickness. This setup is shown in Figure 3-8.

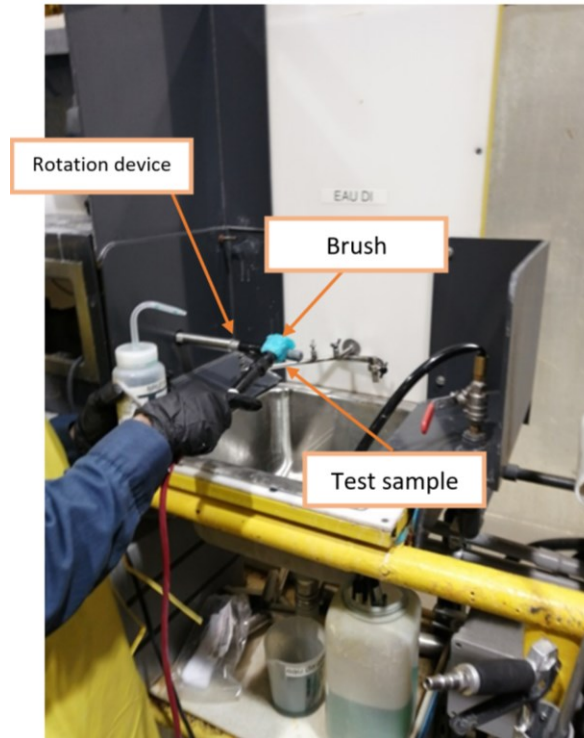


Figure 3-8 Brush plating setup

Table 3-3 summarizes the standard industry plating parameters of the Zn-Ni brush plating procedure as well as the subsequent baking. Applied voltage, which is the controlling parameter, is usually kept constant during the plating process. However, the controlling parameter can be changed from constant voltage to constant current if required. The Alkaline Zn-Ni plating solution was provided by SIFCO ASC and contained ammonium citrate, ammonia, between 15% to 20% Zn sulphate and from 1% to 5% Ni sulphate.

Table 3-3 The industrial brush plating parameters

Parameters	Zn-Ni
Rotation speed (rpm)	60
Voltage (V)	10
Electric charge (A.s)	200
Required thickness (μm)	8-15
Required Ni content (%)	6-20
Baking parameters	24 h at 190°C

Plating is done at 10 V and terminates when 200 A.s of electric charge has been reached which will theoretically deposit a coating of around 11 μm thick. However, this theoretical thickness will not be achieved in practice as will be shown in the next chapter when the average coating thicknesses are measured. Figure 3-9 shows a batch of samples plated with Zn-Ni.



Figure 3-9 Batch of samples plated with Zn-Ni

After plating, the coating thickness as well as the Ni content are measured using a XAN500 Fisherscope XRF (X-Ray Fluorescence) device shown in Figure 3-10 to make sure they are within the designated range. For each sample, the thickness and Ni content are measured twice and the

average values are reported. The standard procedure requires baking to be done within 4 h after plating at a temperature of 190°C for a duration of 24 h.

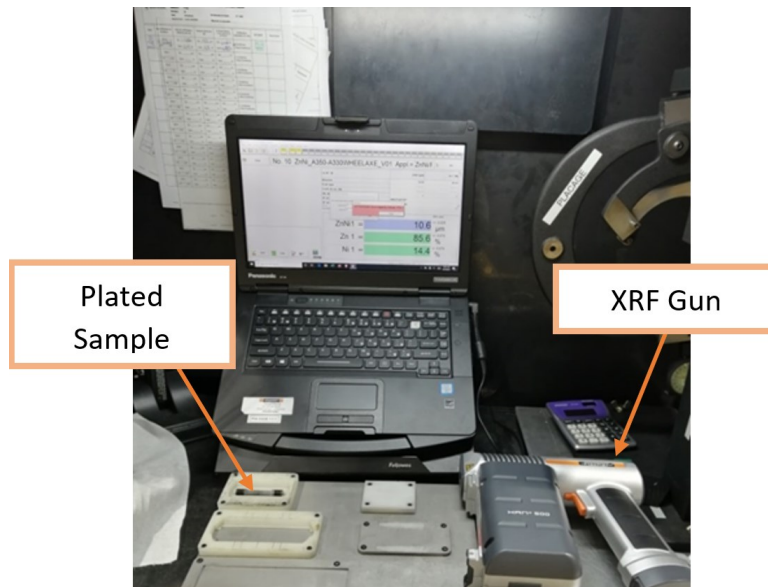


Figure 3-10 The XRF gun used to measure the coating thickness and Ni content

3-4 Sustained load test (SLT) for hydrogen embrittlement evaluation

3-4-1 Test equipment and considerations

SLT is conducted in accordance with ASTM F519 [26] to evaluate HE in electroplated samples. During SLT, type 1a.1 samples are subjected to a sustained tensile load at 75% of the notched fracture strength (NFS) for a duration of 200 h. The NFS of the samples used in this research is 38.59 kN which is the average value obtained from 10 tests conducted by Green Specialties Ltd. Therefore, a sustained tensile load of 28.94 kN (75% of NFS) was applied during SLT. Each test contained a batch of 4 samples fastened to each other using couplings and subsequently mounted in a tensile test setup as shown in Figure 3-11. The tensile test machine used in this study was equipped with a load cell of 50 kN and was programmable to maintain the required applied load for a duration of at least 200 h. In case any of the four samples fractures during the SLT, the test is halted to replace the fractured sample with a dummy sample and then the test is resumed. The replacement dummy samples are shown in Figure 3-12.

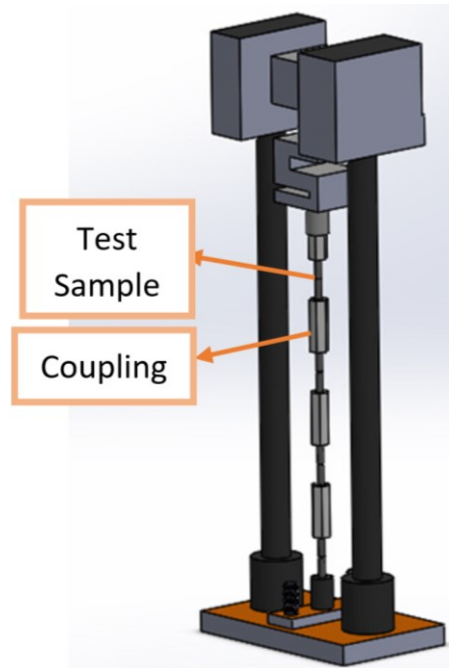


Figure 3-11 A schematic representation of a batch of samples attached to each other and placed in the sustained load test setup



Figure 3-12 Dummy samples used to replace fractured samples in SLT

3-4-2 Evaluation of the sustained load test results

The evaluation of the SLT results is done as follows:

- 1- If none of the 4 samples break within the 200 h test, the samples are considered to be non-embrittled.

- 2- If one of the samples breaks during the 200 h test, the remaining three samples are subjected to a step load test in which the tensile load is increased from 75% to 90% of the NFS in 5% increments that lasts 2 h each. If the three samples survive this test, they are considered non-embrittled.
- 3- The fracture of two or more samples within the 200 h test indicates embrittlement.

After SLT, the fracture surfaces of the samples were analyzed with a Hitachi 3400N SEM in order to locate the fracture origin and analyze the important features on the fracture surface. Further, if required, the elemental analysis of the fracture surface using energy dispersive spectroscope (EDS) was also conducted. The experiments carried out in this research were divided into four categories analyzing the following criteria:

- 1- Effect of baking after brush plating
- 2- Influence of different current densities on HE
- 3- HE severity if coating thickness is reduced and plating is ended before 200 A.s of electric charge
- 4- The influence of pre-plating sandblasting on HE results

Chapter 4 : Results and Discussion

4-1 Results of the sustained load test

Tables 4-1 to 4-4 show the SLT results of the tests that analyzed the influence of baking, plating current density, coating thickness and sandblasting on HE of the substrate metal, respectively. The samples in the first set of experiments (Tests 1-4) were sandblasted and plated with the standard parameters mentioned in Chapter 3 (i.e. 10 V, 200 A.s) but baked under different baking conditions as listed in Table 4-1. In the case of the second set of experiments (Tests 5-8), the samples were sandblasted but plated at different current densities instead of a fixed voltage and no subsequent baking was carried out on them. The current densities were obtained by dividing the plating current by the surface area to be plated which is 1.2 cm². For the third set of experiments (Tests 9-13), samples were sandblasted and plated at 10 V and plating was stopped at 175, 150, 125 and 60 A.s of electric charge to progressively reduce the coating thickness. The last experiment in this set (Test 13) was done with a delay of one week to observe how it will affect the SLT result. The samples in tests 5 to 14 were not baked after plating. In the final experiment (Test 14), samples were plated under standard conditions without the prior sandblasting.

Table 4-1 SLT results for 4 experiments with different baking conditions

Test no.	Plating conditions			Average coating thickness (µm)	Average Ni content (wt%)	SLT result	First fracture (h)	Second fracture (h)
	Baking	Voltage (V)	Charge (A.s)					
1	No baking	10	200	10.21	13.35%	Fail	5	11
2	Baked within 4 h	10	200	10.33	13.41%	Pass	-	-
3	Baked after 24 h	10	200	10.16	13.43%	Pass	-	-
4	Baked at 100°C	10	200	10.25	13.37%	Pass	-	-

Table 4-2 SLT results of the samples plated at different constant plating current densities

Test no.	Plating conditions				Average coating thickness (μm)	Average Ni content (wt%)	SLT result	First fracture (h)	Second fracture (h)
	current density (A/cm^2)	Charge (A.s)	Corresponding voltage (V)	Baking condition					
5	0.66	200	2-2.5	No baking	10.87	13.35%	Fail	5	8
6	2.0	200	4.5-5,5	No baking	10.44	13.31%	Fail	3	6
7	3.3	200	8-10	No baking	10.18	13.48%	Fail	6	6
8	5.3	200	11-12	No baking	9.78	13.8%	Fail	4	9

Table 4-3 SLT results of the samples plated up to 175, 150, 125 and 60 A.s

Test no.	Plating conditions			Average thickness (µm)	Average Ni content (%)	SLT result	First fracture (h)	Second fracture (h)
	Charge (A.s)	Voltage (V)	Baking condition					
9	175	10	No baking	9.77	13.65	Fail	6	9
10	150	10	No baking	9.61	13.67	Fail	6	7
11	125	10	No baking	8.65	13.95	Fail	3	6
12	60	10	No baking	3.17	16.00	Fail	75	175
13	60 (Tested after 1 week)	10	No baking	3.26	15.87	Pass	-	-

Table 4-4 SLT results of the sample plated without sandblasting

Test no.	Plating conditions				Thickness (µm)	Ni content (wt%)	SLT result	First fracture (h)	Second fracture (h)
	Sandblasting	Voltage (V)	Charge (A.s)	Baking conditions					
14	No blasting	10	200	No baking	7.08	14.3	Pass	80	-

4-1-1 Analysis of the sustained load test results

The SLT results show a severe embrittlement of the samples (i.e. end of the SLT before 20 h) under standard plating conditions without baking as evidenced by Test 1. On the other hand, the response to baking is excellent. Not only did the samples pass the SLT after a standard industry baking (Test 2 i.e. baking within 4 h of plating at 190°C) but baking after a delay of 24 h (Test 3) or at a considerably reduced temperature of 100°C (Test 4) also relieved embrittlement. This demonstrates that it is not necessary to follow the industry baking standard for HE relief. This flexibility is important considering that brush plating is often carried out for repair purposes and baking the repaired parts at 190°C could damage the paint on them. Surprisingly, changing the plating parameters did not affect the severity of HE. This will be further elaborated when the coating morphologies and characteristics are discussed in section 4-1-2.

Moreover, another surprising observation was the fact that HE severity did not change whatsoever even if plating is terminated at 125 A.s instead of the standard 200 A.s. The average coating thickness of the samples whose plating ended at 125 A.s is barely above the minimum requirement of 8 μm . However, their embrittlement was just as severe in tests in which plating terminated at 200 A.s and the same applied to tests in which plating ended at 175 A.s and 150 A.s as well. Based on the results reported by Bellemare et al. [76], the threshold hydrogen content for embrittlement to occur was reported to be very low at 0.1 ppm. Thus, it can be concluded that even if plating is ended immediately after minimum coating thickness is achieved, the hydrogen content in the samples has far surpassed the HE threshold. Even when plating ends at 60 A.s, sufficient hydrogen has diffused into the samples to result in the failure of the test albeit after 175 h. However, when the same samples are stored at room temperature for one week before testing, the results change and they pass the test. This is an indication that hydrogen diffuses out of the samples even at room temperature which is a phenomenon that is also reported in the literature [76,83]. However, it is important to consider that the thickness of the coatings in these two tests was well below the required 8 μm (i.e. 3.17 and 3.26 μm). In the case of samples with a much thicker coating, the outward diffusion of hydrogen at room temperature is much more difficult in addition to the hydrogen content being higher as well. Therefore, a much longer delay between plating and the SLT would be required to see a noticeable change in the SLT results.

The Ni content of the coating seems to increase when coating thickness is reduced. This is an indication that the electro-plating process begins with the deposition of a Ni-rich layer of coating and the Ni content drops as the coating becomes thicker. This can further be proven using an EDS analysis to obtain the Ni content of the coating at its interface with the substrate and away from it. Figure 4-1 shows an SEM image of a coating plated under standard conditions and the EDS analysis of the two marked points are brought in Table 4-5. The existence of a Ni-rich layer at the interface of the coating and substrate is in accordance with the literature [66,77]. However, in the case of the Zn-Ni coating in this research, it is clear that the diffusion of hydrogen into the substrate was not impeded by the Ni-rich layer at the coating/substrate interface as opposed to what is reported by Hillier et al. [77]. Analysis of the coating morphology and characteristics in section 4-1-2 will reveal more insights as to why that is the case.

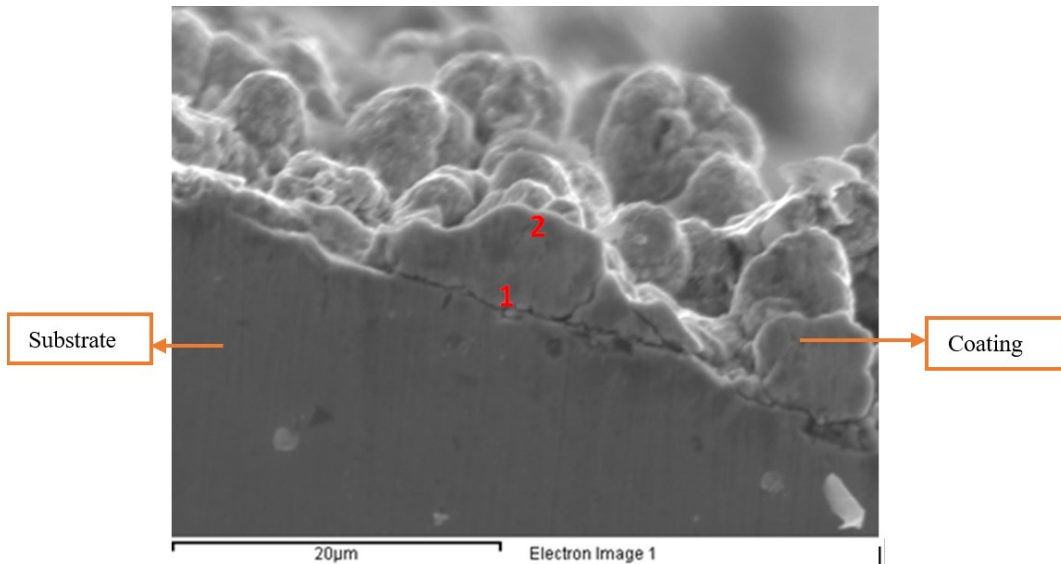


Figure 4-1 Image of the Zn-Ni coating showing the two spots on the coating marked for elemental analysis

Table 4-5- Elemental analysis of the two spots marked in figure 4-1

Element	Point 1 (%wt)	Point 2 (%wt)
Ni	16.64	11.27
Zn	74.82	84.36
Fe	5.96	3.10
C	2.58	1.27

Lastly, sandblasting seems to affect the results of the SLT. As shown in Table 4-4, samples without sandblasting passed the SLT with only one fracture in the SLT and no fractures in the subsequent step load test. This will be further discussed in section 4-1-3. The experiments in this research were conducted at least twice to ensure the repeatability of the results.

4-1-2 Coating morphology and characteristics

As discussed in the previous section, the samples without baking are severely embrittled while showing a complete embrittlement relief even if baked at lower temperatures. Microscopic observations of the coating could provide an explanation for this phenomenon. Figure 4-2 shows the change in coating morphology with increase in plating current density. The coating has a platelet-like morphology similar to what is reported by Conde et al. [59] and Rajagopalan et al. [65]. The platelets also become smaller as plating current density increases. Table 4-6 illustrates the average platelet size for each coating which is measured by calculating the average of 10 measurement for each coating. This decrease in platelet size is due to the fact that increase in plating current density increases the nucleation rate of the platelets thus making them smaller in size [89,90].

Another characteristic of the coatings is the existence of intermittent gaps and pinholes between the platelets some of which are marked in Figure 4-2. An SEM image of the coating of one of the samples plated under standard conditions is shown in Figure 4-3 demonstrating similar noticeable gaps and pinholes on the coating surface. Moreover, visible micro-cracks and discontinuities also exist across the thickness of the coating as demonstrated in Figure 4-4.

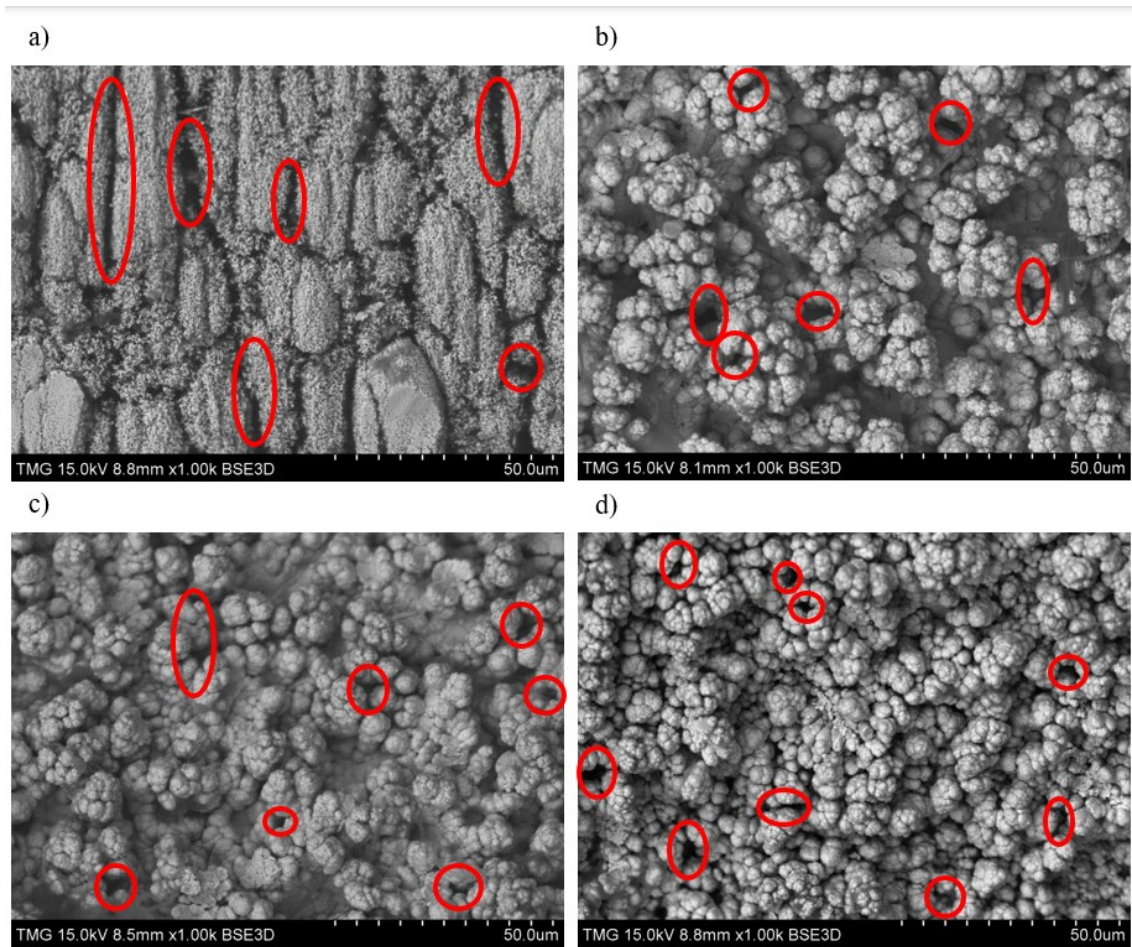


Figure 4-2 Evolution of coating morphology showing samples plated at a) 0.66 A/cm² b) 2.0 A/cm² c) 3.3 A/cm² d) 5.3 A/cm²

Table 4-6 Change in platelet size with variation in plating current density

Plating current density (A/cm ²)	Average platelet size (µm)
0.66	12.35 ± 0.8
2.0	5.80 ± 0.5
3.3	3.67 ± 0.5
5.3	2.50 ± 0.3

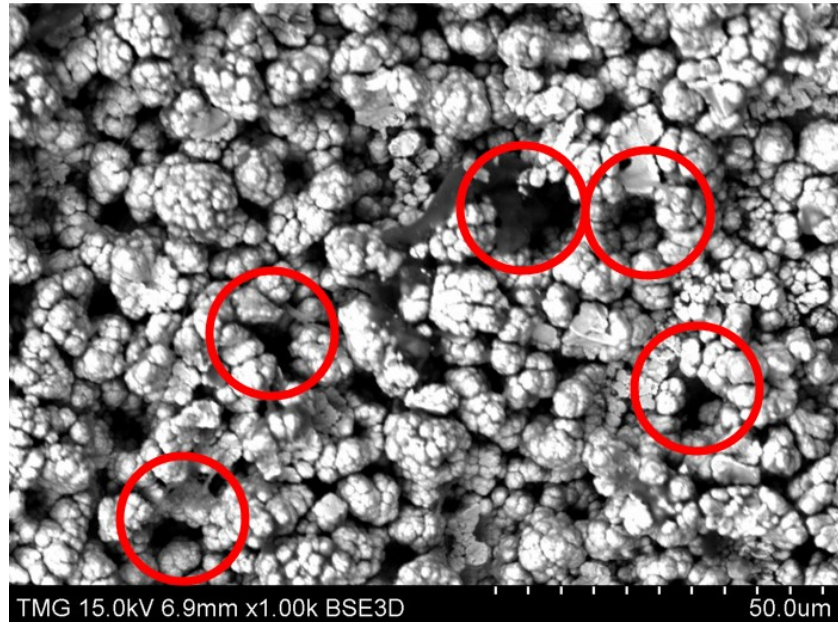


Figure 4-3 Coating morphology of a sample plated with standard plating parameters

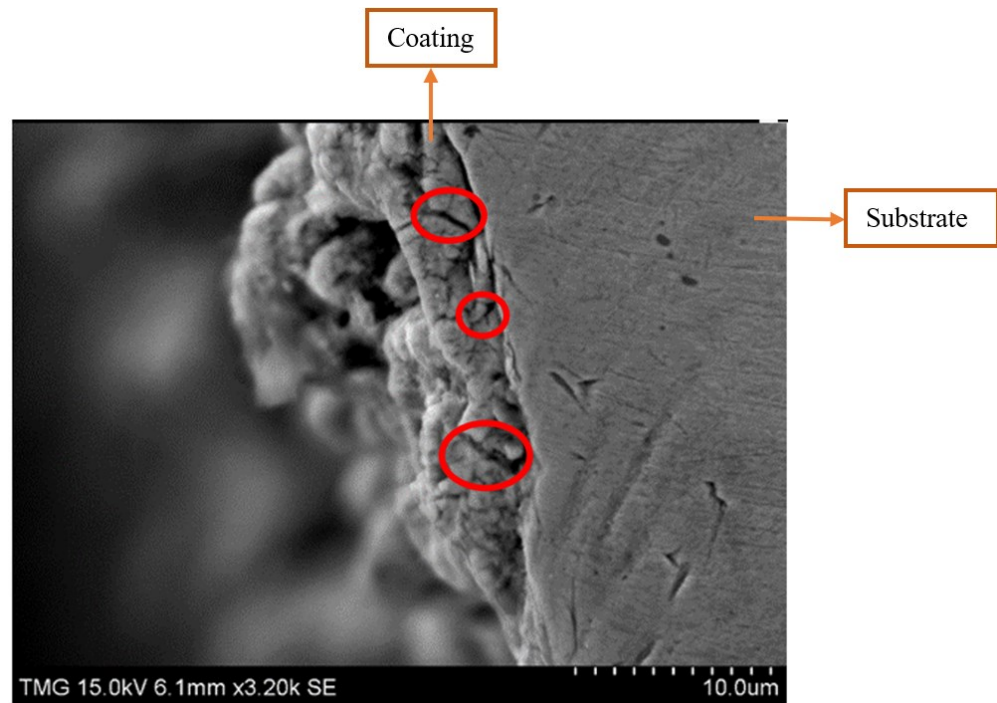


Figure 4-4 Cross sectional image of a sample where through thickness micro-cracks in the coating are visible

The existence of the aforementioned features significantly facilitates the diffusion of hydrogen through the coating as discussed in the chapter 2. Therefore, hydrogen can easily diffuse into the samples during plating and subsequently diffuse out of them during the baking. This explains why

embrittlement is so severe despite the presence of a Ni-rich layer at the interface while even baking at a lower temperature is sufficient for embrittlement relief.

4-1-3 The effect of sandblasting

The pre-plating sandblasting procedure created a uniform surface roughness on the samples but left noticeable alumina (Al_2O_3) residue. Figure 4-5 shows the SEM micrograph of the notch of a sandblasted sample with alumina residue particles on it and the elemental analysis spectra of spots marked as 1, 2 and 3 are shown in Figures 4-6, 4-7 and 4-8 respectively. The atomic percentages of the elements of each analysis are shown in Table 4-7 indicating the presence of alumina on specimen surface after sandblasting. Further, Figure 4-9 shows the low magnification SEM micrograph of the notched sample to better demonstrate the spread of sandblasting residue on the surface as well as the notch root of the sample.

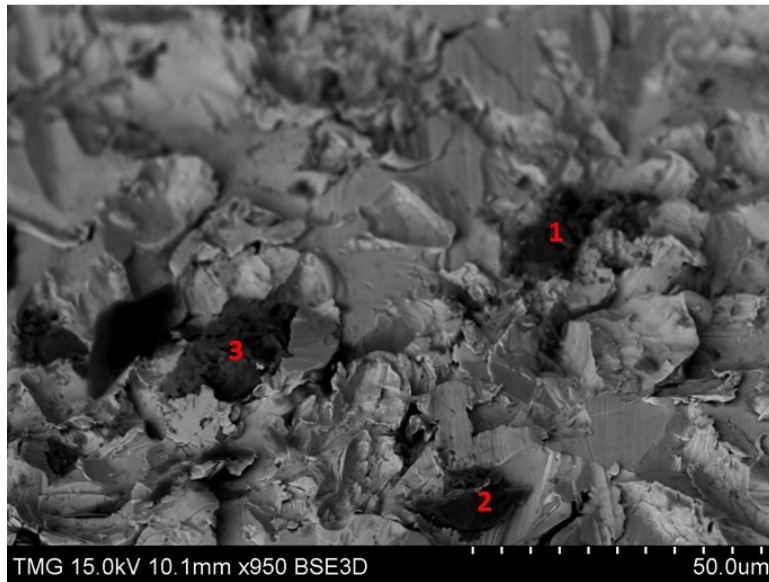


Figure 4-5 SEM micrograph at the notch of a sample after sandblasting showing 3 alumina residue particles marked for EDS and elemental analysis

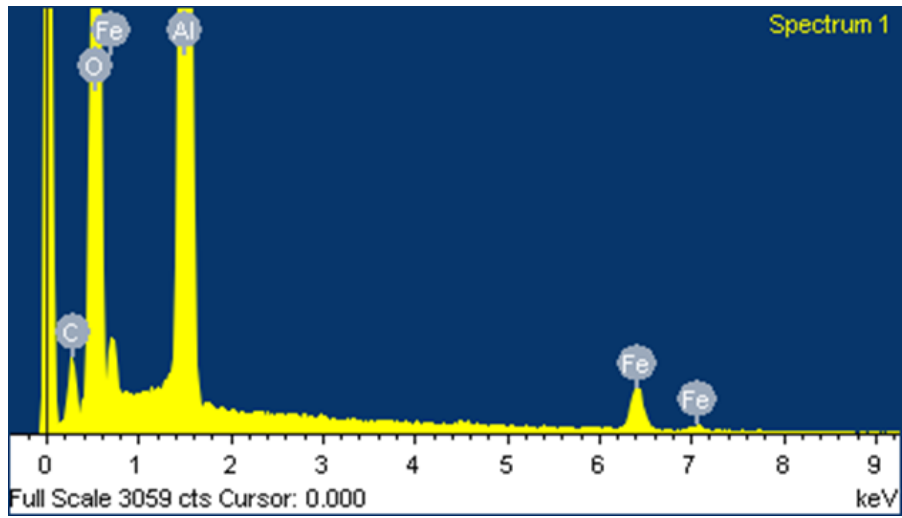


Figure 4-6 EDS analysis of particle 1 in figure 4-5

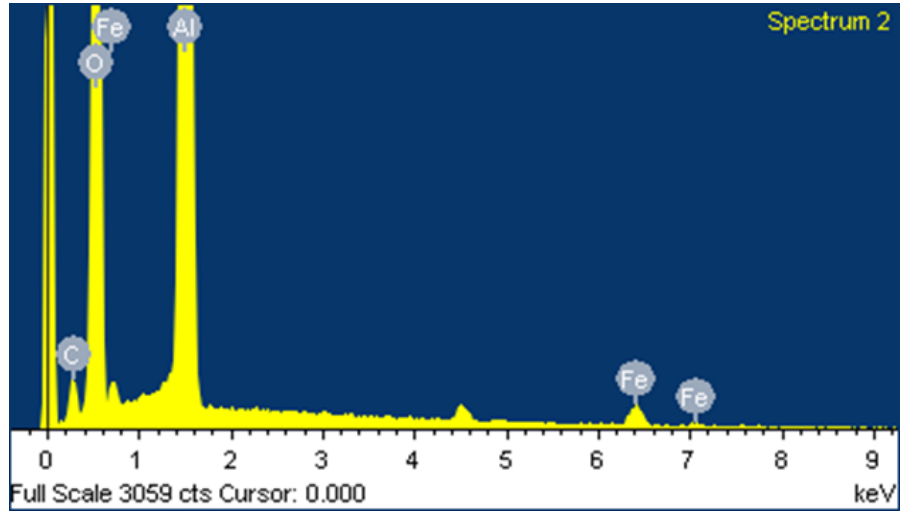


Figure 4-7 EDS analysis of particle 2 in figure 4-5

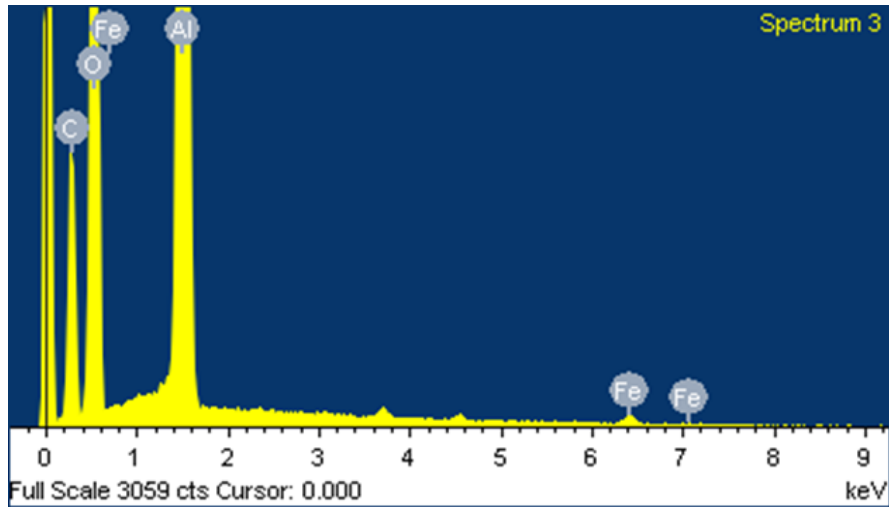


Figure 4-8 EDS analysis of particle 3 in figure 4-5

Table 4-7 Elemental analysis of the three points marked as 1, 2 and 3 in figure 4-5

Element	Spectrum 1 (%at)	Spectrum 2 (at%)	Spectrum 3 (at%)
Al	37.94	34.18	27.60
O	46.33	56.62	54.77
Fe	0.74	0.75	0.24
C	14.98	7.45	17.39

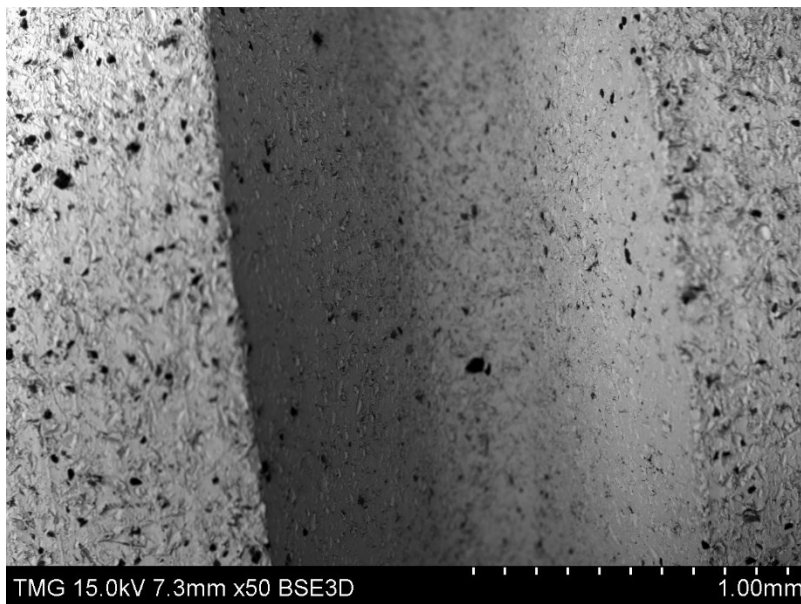


Figure 4-9 SEM image of the notch and surrounding areas of a sandblasted samples showing the visible residual alumina at low magnification

The substantial alumina residue on the samples suggests that the sandblasting might have been severe which could introduce surface defects that can facilitate fracture especially in a notched sample. This can be better demonstrated by observing the notch roots after SLT. Figure 4-10 shows the notch root images of a sandblasted sample prior to plating with visible cracks on it. Figure 4-11 shows the depth of the cracks on the notch root. Figure 4-12 shows the same sample with its coating stripped in which the cracks can still be seen on the notch. The stripping processing was done using ammonium hydroxide (NH_4OH) as the stripping solution and the sample was stress relieved at 190°C for 4 h to ensure that the cracks are not the result of residual stresses. Therefore, it can safely be concluded that sandblasting increases the risk of fracture during the SLT. Evidently, the adhesion of the coating is noticeably worse for the sample without sandblasting. Thus, the parameters of sandblasting should be optimized to mitigate the risk of failure as much as possible while also providing an adequate adhesion between the coating and the substrate. It is also possible to completely replace sandblasting with another surface preparation measure such as grinding with an abrasive as recommended in the literature [91].

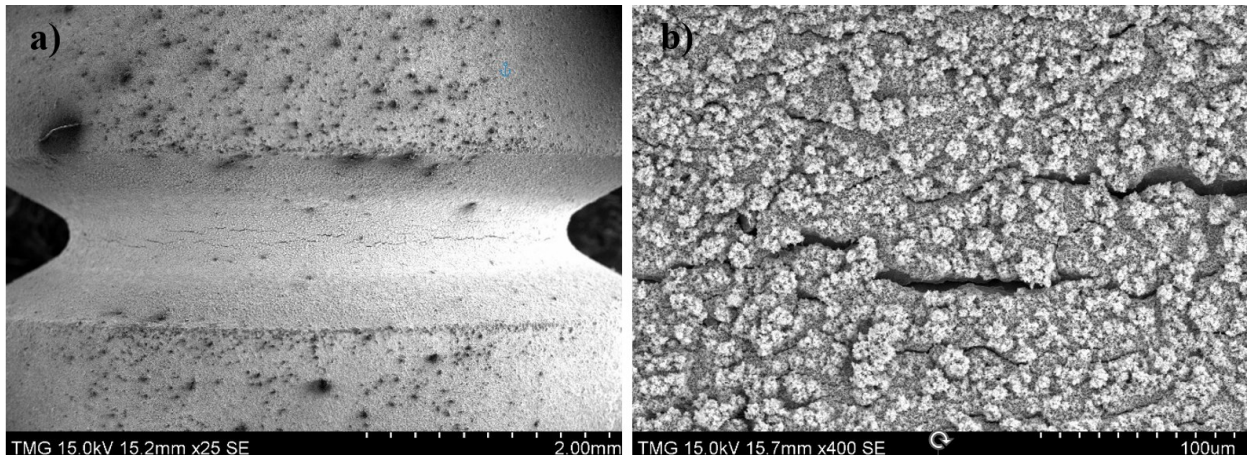


Figure 4-10 SEM image of the notch of a sandblasted sample plated with standard plating parameters after the end of the SLT showing a) the existence of cracks on the notch b) a higher magnification image to better show the presence of deep cracks

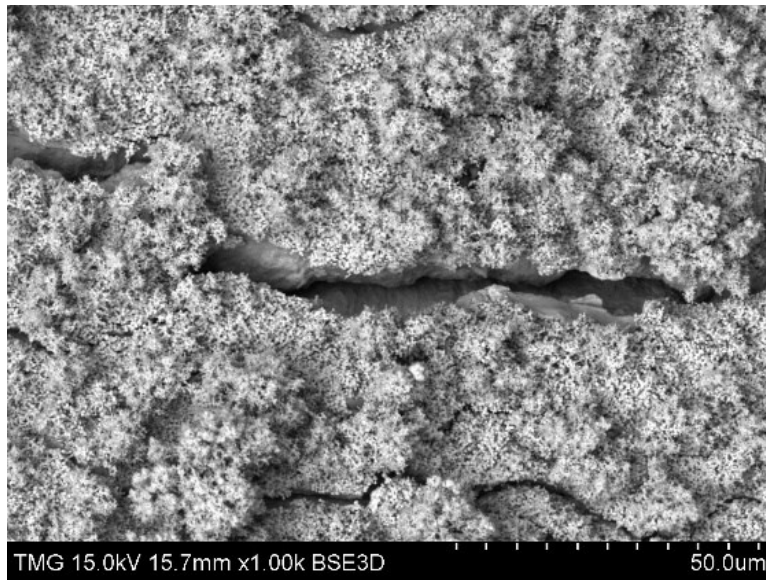


Figure 4-11 SEM image of the cracks in figure 4-10b demonstrating their depth

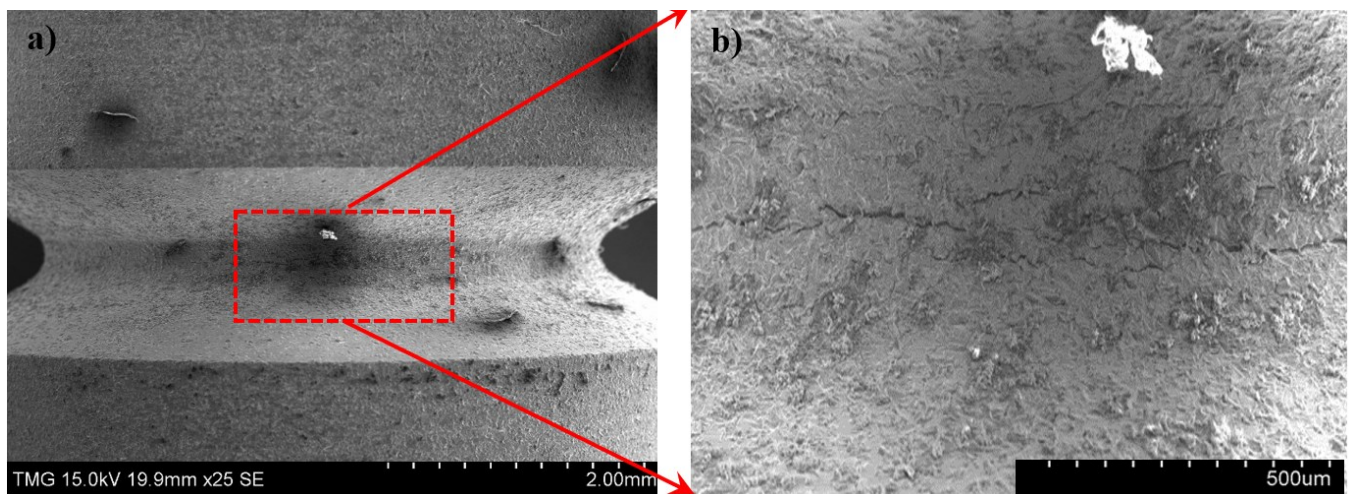


Figure 4-12 SEM image of the notch of the sample in Figure 4-10 after its coating was stripped showing a) the notch b) a higher magnification image of the notch to better show the cracks

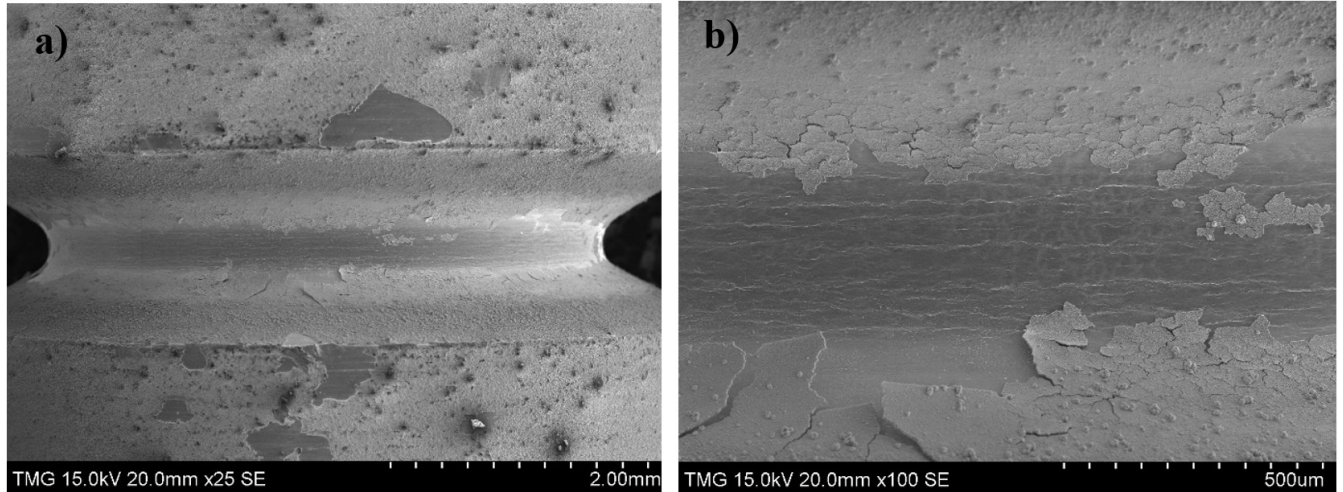


Figure 4-13 image of the notch of a sample without sandblasting and plated with standard plating parameters after the end of the SLT showing a) the notch b) a higher magnification image of the notch to better demonstrate the absence of cracks

4-2 Fracture surface analysis

Fractography of the embrittled samples revealed a combination of ductile features in the form of dimples and micro-voids and brittle features in the form of intergranular fracture. Figure 4-14 shows SEM images of the fracture surface of one of the fractured samples that were plated under standard conditions without baking. At a low magnification, ridge patterns can be seen on the fracture surface of the specimen that converge towards the edge of the fracture surface (Figure 4-14a). This indicates the region from which the main crack must have initiated. Upon focusing on this area, intergranular fracture features were observed (Figure 4-14b). The presence of these intergranular features is a manifestation of the HEDE mechanism that was described in chapter 2. Dimples and micro-voids can also be seen alongside intergranular fracture. However, away from this fracture initiation region as shown in Figure 4-14c, dimples and surface features associated with ductility such as micro-voids begin to overtake the brittle intergranular fracture features. Further, towards the center of the fracture surface as shown in Figure 4-14d, the intergranular features completely disappear and fracture was dominated by dimples and micro-void coalescence. It should also be noted that intergranular features were not observed anywhere else on the surface and they were only seen in the crack initiation region at the edge of the fracture surface. This is expected considering that hydrogen content is higher at the interface of the coating and the substrate compared to the center of the specimen [92]. Thus, intergranular fracture is expected to occur at the edge rather than at the center.

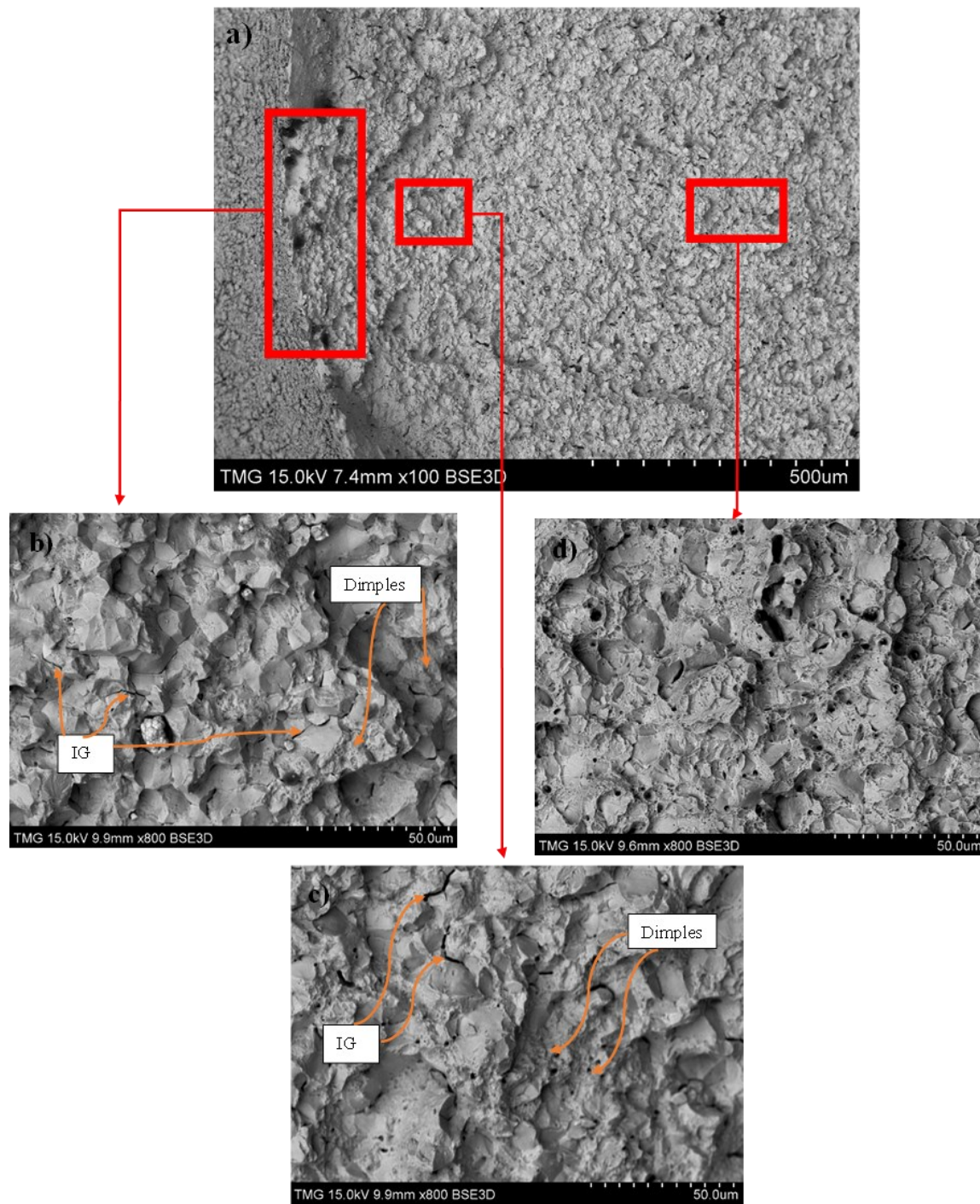


Figure 4-14 SEM image of the surface of the first fractured sample from Test 1 showing a) fracture initiation region on the edge of the surface b) intergranular fracture at fracture initiation region c) dimples and ductile features becoming more dominant away from the fracture initiation region d) ductile fracture features at the centre of the fracture surface

The fracture surfaces of some of the other embrittled samples are shown in Figures 4-15 to 4-19 exhibiting similar characteristics. When comparing the fracture initiation regions of the embrittled

samples, it is noticeable that different samples have varying degrees of mixture of intergranular and ductile features in their fracture initiation regions. For example, the sample in Figure 4-17 has a visibly more mixed fracture initiation region compared to that in figure 4-14. However, all of these samples showed similar levels of embrittlement severity and they all failed very early in their SLT cycles. Therefore, the existence of more ductile features alongside intergranular features has no bearing on the severity of embrittlement and does not indicate less embrittlement. It must be noted that many HE mechanisms such as HELP, HESIV and AIDE manifest themselves in the form of dimples and micro-voids on the fracture surface as discussed in chapter 2 and work in synergy with each other [48,54,55]. Therefore, it is plausible to assume that fracture has occurred through a combination of HEDE and other HE mechanisms.

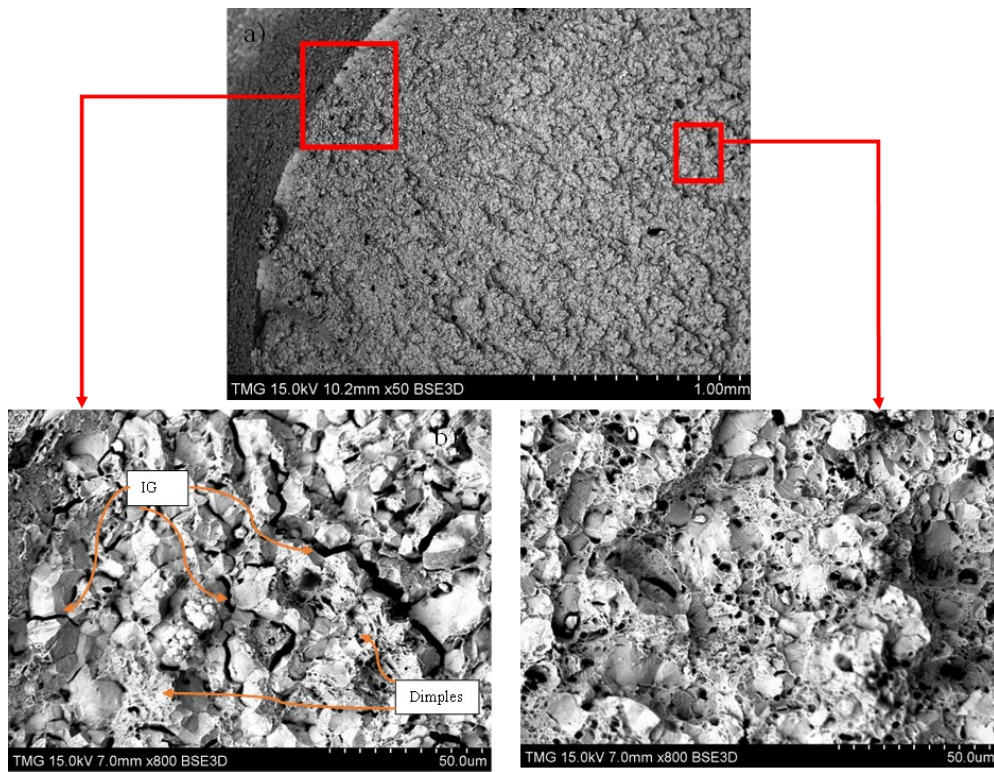


Figure 4-15 SEM images of the surface of the second fractured sample from Test 1 showing a) fracture initiation region on the edge of the surface b) intergranular fracture at fracture initiation region accompanied by dimples and voids c) ductile features away from the fracture initiation region

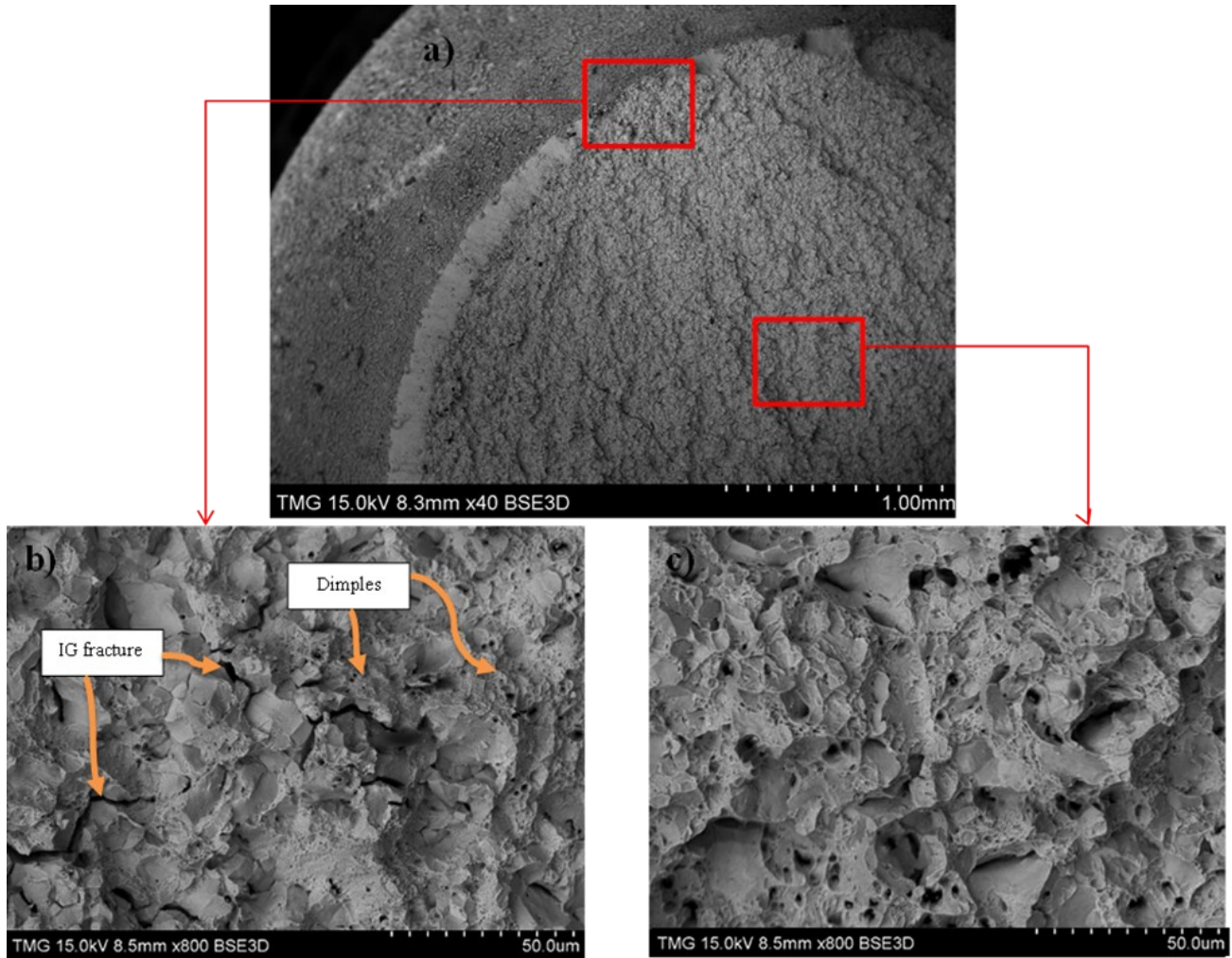


Figure 4-16 Fracture surface of the first fractured sample from Test 6 showing a) fracture initiation region on the edge of the surface b) intergranular features at fracture initiation region c) ductile fracture surface away from the fracture initiation region

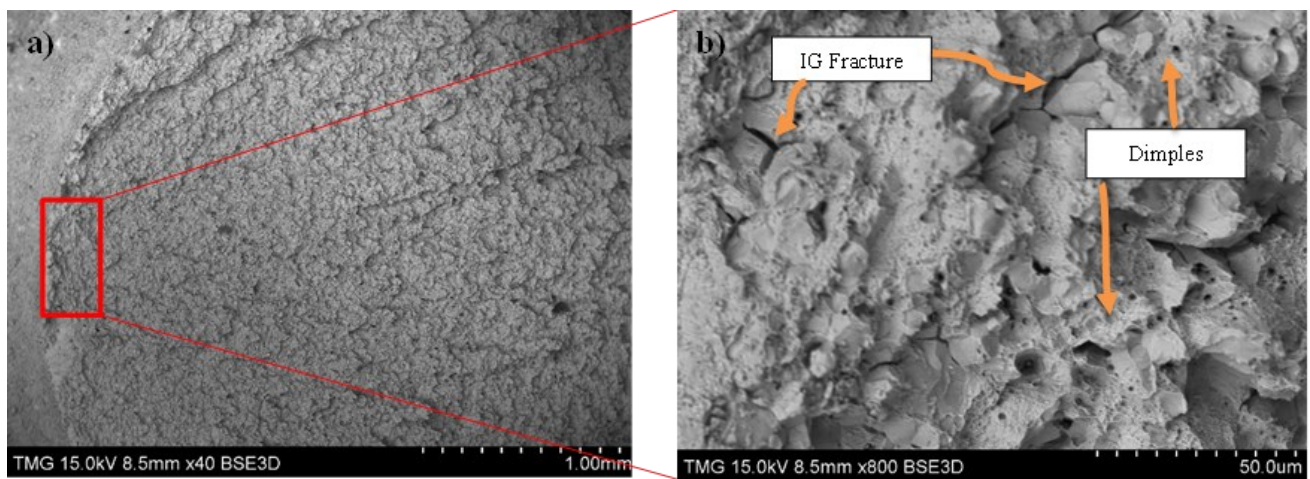


Figure 4-17 Fracture surface of the second fractured sample of Test 6 showing a) the fracture initiation region and b) the intergranular fracture alongside ductile dimples at the fracture initiation region

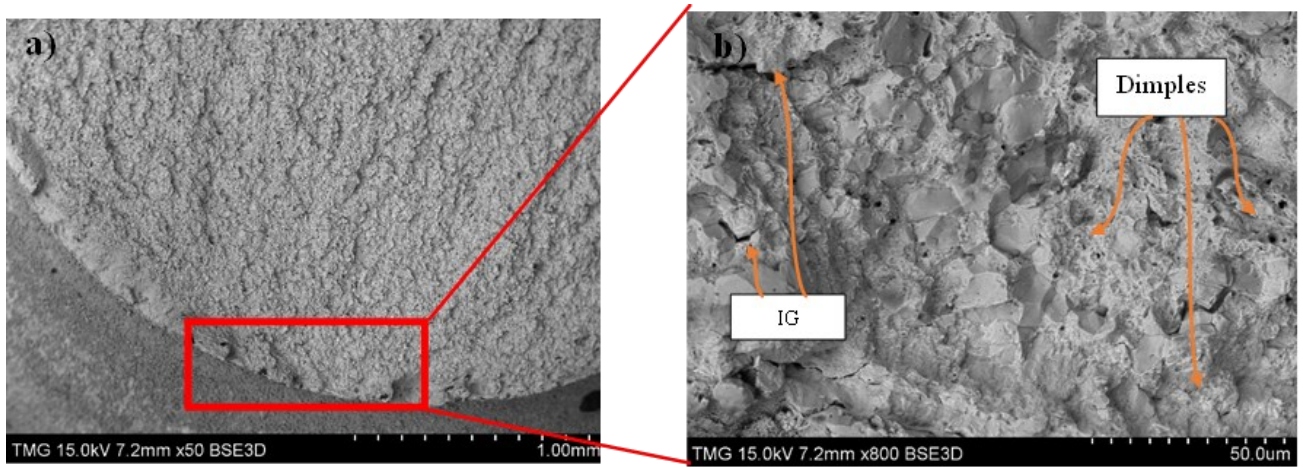


Figure 4-18 Fracture surface of the first fractured sample of Test 7 showing a) the fracture initiation region and b) the intergranular fracture alongside ductile dimples at the fracture initiation region

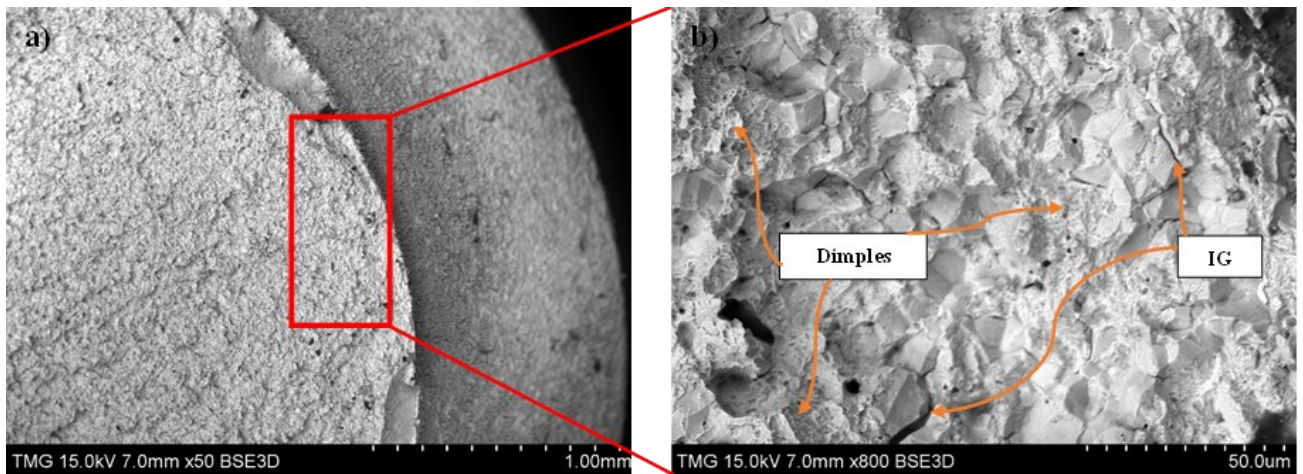


Figure 4-19 Fracture surface of the second fractured sample from Test 7 showing a) the fracture initiation region and b) the intergranular fracture alongside ductile dimples at the fracture initiation region

Chapter 5 : Conclusions and future directions

5-1 Conclusions

The present thesis studied the HE susceptibility of Zn-Ni brush plating. The standard industry procedure of this process requires a pre-plating sandblasting for surface preparation, plating at a fixed voltage of 10 V up to a total electric charge of 200 A.s and a subsequent baking at 190°C for 24 h. SLTs with 14 different plating conditions were carried out in order to evaluate the influence of baking, plating current density, reduction in coating thickness and sandblasting on HE susceptibility of Zn-Ni brush plating. Subsequent fracture surface analyses were carried out to investigate the cause of failure. Overall, the conclusions of this research can be divided into the following three categories:

5-1-1 Conclusions derived from HE evaluation

1. The standard plating parameters without baking cause severe HE. The SLT test failed within 11 h. Whereas, standard industrial baking process carried out just after plating completely relieves HE.
2. Baking with a delay of 24 h also relieved HE. More importantly, baking at a much lower temperature of 100°C instead of the standard 190°C fully relieved HE as well.
3. Changing the plating current density (from 0.66 to 5.4 A/cm²) had no effect on the HE susceptibility of the current Zn-Ni brush plating process. Samples plated at different current densities up to a charge of 200 A.s failed similarly during SLT.
4. Surprisingly, HE severity did not change when plating even at the minimum required coating thickness.
5. SLT results substantially improved by skipping the pre-plating sandblasting. The samples without sandblasting passed the SLT while sandblasted samples failed

5-1-2 Conclusions derived from microscopic observations of the fracture surfaces

1. Intergranular fracture was observed for every fractured sample at the fracture initiation region.
2. Dimples and micro-voids also accompanied the intergranular features at the fracture initiation regions of embrittled samples.
3. The existence of ductile features such as dimples in the fracture initiation region does not indicate that the embrittlement is less severe as samples with varying degrees of ductility in their fracture initiation region failed the SLT after a similar time.

5-1-3 Conclusions from secondary observations

1. The morphology of the coatings resembled platelets agglomerated with each other. These platelets became smaller in size with the increase in the plating current density.
2. Gaps between the platelets on the coating surface as well as micro-cracks along the thickness of the coating were observed. These features considerably facilitate hydrogen diffusion and help explain the desirable baking response.

5-2 Future directions

Brush plating is a process that has not been investigated as thoroughly in the literature as bath plating. Therefore, there are many opportunities to carry out research focused on brush plating.

One such avenue for research would be to investigate the HE susceptibility of different Zn-Ni solutions and the influence of different ingredients as well as different pH on mitigating HE. The addition of hydrogen inhibitors could also be investigated.

Similar research can be done to investigate the HE tendencies of other alloys similar to the SAE 4340 that can be used in landing gears. Although this alloy is the most widely used in landing gear and for the production of samples for the embrittlement tests, there is a range of other alloys with similar compositions designed for similar purposes. Two of these alloys are 300M and Ferrium M54 that are gaining traction in the aerospace industry and investigating their HE susceptibility during the plating process is of great industrial value.

Future research could also extend beyond Zn-Ni coatings. There is a myriad of other coatings such as Zn-Co, Zn-Ti or pure Zn coatings that can be considered as a replacement for Cd. Just like Zn-Ni, the suitability of these coatings for brush plating as well as their HE tendencies should be analyzed.

The effects of sandblasting on the SLT results can be analyzed further. Investigating sandblasting parameters such as alumina particle size and morphology and their effect on increasing the failure risk of the SLT could be of interest. Moreover, analyzing the influence of pre-plating surface preparation steps on the mechanical properties of the notched 1a.1 samples could provide interesting research opportunities.

5-3 Contributions

This work investigated the entirety of an industrial Zn-Ni brush plating procedure and the influence of pre-plating and post-plating operations on the HE of the substrate metal. The possibility of deviation from standard industry practices regarding baking was explored in this research. This is important since flexibility in the baking procedure is needed for brush plating and parts with painting can't be baked at a high temperature. Moreover, the effect of sandblasting on the HE results was analyzed revealing the importance of this pre-plating procedure in HE tests and the necessity to adjust its parameters with care to achieve good coating adhesion but without increasing the embrittlement susceptibility.

References

- [1] W.H. Johnson, “On some remarkable changes produced in iron and steel by the action of hydrogen and acids”, Proceedings of the Royal Society of London, Vol 23, 168 – 180 (1875)
- [2] L.B. Pfeil., “The effect of occluded hydrogen on the tensile strength of iron”, Proceedings of the Royal Society of London, Vol 112, 182-195 (1926)
- [3] M. Morris, M. Bowker, D. King, “Kinetics of adsorption, desorption and diffusion at metal surfaces”, Comprehensive Chemical Kinetics, Vol 19, 1-179 (1984)
- [4] J.R.G. da Silva, S.W. Stafford, R.B. McLellan, “The thermodynamics of the hydrogen-iron system”, Journal of less-common metals, Vol 49, 407-420 (1976)
- [5] A. Sieverts, “The absorption of gases by metals”, International Journal of Materials Research, Vol 21, 37–46 (1929)
- [6] M. Nagumo, “Solid solution”, Fundamentals of hydrogen embrittlement, Springer, Singapore, 1-10 (2016)
- [7] A. Turnbull, “Hydrogen diffusion and trapping in metals”, Gaseous Hydrogen Embrittlement of Materials in Energy Technologies, R.P. Gangloff and B.P. Somerday Eds., Woodhead Publishing Series in Metals and Surface Engineering, Vol 2, 89-128 (2012)
- [8] Y. Fukai, “Hydrogen in alloys”, The Metal-Hydrogen System, Springer Series in Materials Science 2nd ed, Springer, Berlin, Vol 21, 55-90 (2005)
- [9] K. Kiuchi, R.B. McLellan, “The solubility and diffusivity of hydrogen in well annealed and deformed iron”, Acta Metallurgica, Vol 31, 961–984 (1983)
- [10] G. M. Presouyre, “Trap theory of hydrogen embrittlement”, Acta Metallurgica, Vol 28, 895-911 (1980)
- [11] M. Koyama, M. Rohweder, C.C. Tasan, A. Bashir, E. Akiyama, K. Takai, D. Raabe, K. Tsuzaki, “Recent progress in microstructural hydrogen mapping in steels: quantification, kinetic analysis, and multi-scale characterization”, Materials Science and Technology, Vol 33(13), 1481–1496 (2017)

- [12] A. Pundt, R. Kirchheim, “Hydrogen in metals: microstructural aspects”, *Annual Review of Materials Research*, Vol 36, 555 – 608 (2006)
- [13] E. Myoshi, T. Tanaka, F. Terasaki, A. Ikeda, “Hydrogen-Induced Cracking of Steels Under Wet Hydrogen Sulfide Environment”, *Journal of Engineering for Industry*, Vol 98, 1221-1230 (1976)
- [14] Y. Tateyama, T. Ohno, “Stability and clusterization of hydrogen-vacancy complexes in a-Fe: an ab-initio study”, *Physical Review B*, Vol 67, 174105 (2003)
- [15] W. Wallace, D.W. Hoppener, P.V.Kandachar, “Aircraft Corrosion: Causes and Case Histories”, *Agard Corrosion Handbook*, Vol 1, (1985)
- [16] A.A Baker, “Composite Materials for Aircraft Structures”, 2nd ed., American Institute of Aeronautics and Astronautics, Reston, USA, (2004)
- [17] A.D. Dayan, A.J. Paine, “Mechanisms of chromium toxicity, carcinogenicity and allergenicity: review of the literature from 1985 to 2000”, *Human & Experimental Toxicology*, Vol 20, 439–451 (2001)
- [18] M.P. Waalkes, “Cadmium carcinogenesis”, *Mutation Research/Fundamental and Molecular Mechanisms of Mutagenesis*, Vol 533, 107-120 (2003)
- [19] B. Navinšek, P. Panjan, I. Milošev, “PVD coatings as an environmentally clean alternative to electroplating and electroless processes”, *Surface and Coatings Technology*, Vol 116-119, 476-487 (1999)
- [20] J.P. Hirth, “Effects of hydrogen on the properties of iron and steel”, *Metallurgical Transactions A*, Vol 11, 861–890 (1980)
- [21] D. Hardie, E.A. Charles, A.H. Lopez, “Hydrogen embrittlement of high strength pipeline steels”, *Corrosion Science*, Vol 48, 4378-4385 (2006)
- [22] A. Kishi, N. Takano, “Effect of hydrogen cathodic charging on fatigue fracture of type 310S stainless steel”, *Journal of Physics: Conference Series*, Vol 240, 012050 (2010)

- [23] A.V. Bochkaryova, Y.V. Li, S.A. Barannikova, L.B Zuev, “The effect of hydrogen embrittlement on the mechanical properties of aluminum alloy”, IOP Conference Series: Materials Science and Engineering, Vol 71, 012057 (2015)
- [24] I.M. Robertson, P. Sofronis, A. Nagao, M.L. Martin, S. Wang, D.W. Gross, K.E. Nygren, “Hydrogen embrittlement understood”, Metallurgical and Materials Transactions B, Vol 46, 1085-1103 (2015)
- [25] M.B. Djukic, G.M. Bakic, V.S. Zeravcic, A. Sedmak, B. Rajicic, “Hydrogen embrittlement of industrial components: prediction, prevention, and models”, Corrosion, Vol 72, 943-961 (2016)
- [26] “ASTM F519: Standard Test Method for Mechanical Hydrogen Embrittlement Evaluation of Plating/Coating Processes and Service Environments”, ASTM International, West Conshohocken, PA, USA, ASTM International (2018)
- [27] N. Eliaz, A. Shachar, B. Tal, D. Eliezer, “Characteristics of hydrogen embrittlement, stress corrosion cracking and tempered martensite embrittlement in high-strength steels”, Engineering Failure Analysis, Vol 9, 167-184 (2002)
- [27] E. Pouillier, A.F. Gourgues, D. Tanguy, E.P. Busso, “A study of intergranular fracture in an aluminium alloy due to hydrogen embrittlement”, International Journal of Plasticity, Vol 34, 139-153 (2012)
- [28] L. Zhenguang, G. Xiuhua, D. Linxiu, L. Jianping, Z. Xiaowei, W. Xiaonan, W. Yuxin, L. Chuan, X. Guoxiang, R.D.K. Misra,” Hydrogen assisted cracking and CO₂ corrosion behaviors of low-alloy steel with high strength used for armor layer of flexible pipe”, Applied Surface Science, Vol 440, 974-991 (2018)
- [29] S. Laliberté-Riverin, J. Bellemare, F. Sirois, M. Brochu, “Determination of hydrogen embrittlement stress intensity threshold by fractography”, Materialia, Vol 12 (2020)
- [30] S.P. Lynch, “Metallographic and fractographic techniques for characterising and understanding hydrogen-assisted cracking of metals”, Gaseous Hydrogen Embrittlement of Materials in Energy Technologies, R. Gangloff and B. Somerdey Eds., Woodhead Publishing Series, Vol 2, 274-346 (2012)

- [31] C.A Zapffe, C.E. Sims, “Hydrogen embrittlement, internal stress and defects in steel”, Transactions of the American Institute of Mining and Metallurgical Engineers, Vol 145, 225-271 (1941)
- [32] C.D. Beachem, “A new model for hydrogen assisted cracking (Hydrogen embrittlement)”, Metallurgical Transactions, Vol 3, 441 – 455 (1972)
- [33] M. Watanabe, “Transmission Electron Microscopy”, Materials Characterization, 2019 ed., ASM Handbook, ASM International, Vol 10, 592-613 (2019)
- [34] Y.N. Picard, “Scanning Electron Microscopy”, Materials Characterization, 2019 ed., ASM Handbook, ASM International, Vol 10, 543-575 (2019)
- [35] M.B. Djukic, G.M. Bakic, V.S. Zeravcic, A. Sedmak, B. Rajcic, “The synergistic action and interplay of hydrogen embrittlement mechanisms in steels and iron: Localized plasticity and decohesion”, Engineering Fracture Mechanics, Vol 216, 106528 (2019)
- [36] S.P. Lynch, “Mechanisms of hydrogen assisted cracking – a review”, Hydrogen effects on materials behavior and corrosion deformation interactions, N.R. Moody, A.W. Thompson, R.E. Ricker, G.W. Was, R.H. Jones Eds., The Minerals, Metals and Materials Society, 449 – 466 (2003)
- [37] Y. Zhao, M.Y. Seok, I.C. Choi, Y.H. Lee, S.J. Park, U. Ramamurty J.U. Suh, J.I. Jang, “The role of hydrogen in hardening/softening steel: Influence of the charging process”, Scripta Materiala, Vol 107, 46–49 (2015)
- [38] A.R. Troiano, “The role of hydrogen and other interstitials in the mechanical behavior of metals”, Metallography, Microstructure, and Analysis, Vol 5, 557–569 (2016)
- [39] R.A. Oriani, “A mechanistic theory of hydrogen embrittlement of steels”, Physical Chemistry, Vol 76, 848 – 857 (1972)
- [40] H.K. Birnbaum, P. Sofronis, “Hydrogen-enhanced localized plasticity – a mechanism for hydrogen-related fracture”, Materials Science and Engineering A, Vol 176, 191 – 202 (1994)

- [41] I.M. Robertson, H.K. Birnbaum, and P. Sofronis, “Hydrogen Effects on Plasticity”, *Dislocations in Solids*, J.P. Hirth and L. Kubin Eds., Elsevier, New York, Vol 15, 249-293 (2009)
- [42] D.G. Westlake, “The habit planes of zirconium hydride in zirconium and zircaloy”, *Journal of Nuclear Materials*, Vol. 26, 208–216 (1968)
- [43] H.K. Birnbaum, “Mechanisms of hydrogen related fracture of metals”, Technical report, Illinois University at Urbana Department of Materials Science and Engineering (1989)
- [44] S.P. Lynch, “Comments on a unified model of environment-assisted cracking”, *Scripta Materiala*, Vol 61, 331 – 334 (2009)
- [45] M. Nagumo, K. Takai, “The predominant role of strain-induced vacancies in hydrogen embrittlement of steels: Overview”, *Acta Materiala*, Vol 165, 722-733 (2019)
- [46] P. Sofronis, I. Robertson, “Viable Mechanisms of Hydrogen Embrittlement—A Review”, *AIP Conference Proceedings*, Vol 837, 64-70 (2006)
- [47] M. Wada, N. Akaiwa, T. Mori, “Field evaporation of iron in neon and hydrogen and its rate-controlling processes”, *Philosophical Magazine A*, Vol 55, 389 – 403 (1987)
- [48] S.P. Lynch, “Hydrogen embrittlement phenomena and mechanisms”, *Corrosion Reviews*, Vol 30, 105–123 (2012)
- [49] D.S. Shih, I.M. Robertson, H.K. Birnbaum, “Hydrogen embrittlement of alpha titanium: in situ TEM studies”, *Acta Metallurgica*, Vol 36, 111-124 (1988)
- [50] Y. Murakami, T. Kanezaki, Y. Mine, “Hydrogen effect against hydrogen embrittlement”, *Metallurgical and Materials Transactions A*, Vol 41(10), 2548–2562 (2010).
- [51] I.H. Katzarov, D.L. Pashov, A.T. Paxton, “Hydrogen embrittlement I. Analysis of hydrogen enhanced localized plasticity: Effect of hydrogen on the velocity of screw dislocations in α Fe”, *Physical Review Materials*, 033602 (2017)

- [52] S. Taketomi, R. Matsumoto, S. Hagihara, “Molecular statics simulation of the effect of hydrogen concentration on $\{112\}\langle 111 \rangle$ edge dislocation mobility in alpha iron”, *ISIJ International*, Vol 57(11), 2058–2064 (2017)
- [53] P. Novak, R. Yuan, B.P. Somerday, P. Sofronis, R.O. Ritchie, “A statistical, physical-based, micro-mechanical model of hydrogen-induced intergranular fracture in steel”, *Journal of the Mechanics and Physics of Solids*, Vol 58(2), 206–226 (2010).
- [54] R. Matsumoto, S. Seki, S. Taketomi, N. Miyazaki, “Hydrogen-related phenomena due to decreases in lattice defect energies-Molecular dynamics simulations using the embedded atom method potential with pseudo-hydrogen effects”, *Computational Materials Science*, Vol 92, 362–371 (2014)
- [55] K.N. Solanki, D.K. Ward, D.J. Bammann, “A nanoscale study of dislocation nucleation at the crack tip in the nickel-hydrogen system”, *Metallurgical and Materials Transactions A*, Vol 42(2), 340–347 (2011)
- [56] K.R. Baldwin, C.J.E. Smith, “Advances in replacements for cadmium plating in aerospace applications”, *Transactions of the Institute of Metal Finishing*, Vol 74, 202–209 (1996)
- [57] M. Ferreira Fernandes, J.R.M. dos Santos, V.M. de Oliveira Velloso, H.J.C. Voorwald, “AISI 4140 steel fatigue performance: cd replacement by electroplated Zn-Ni alloy coating”, *Journal of Materials Engineering and Performance*, Vol 29, 1567–1578 (2020)
- [58] P. Ganesan, S.P. Kumaraguru, B.N. Popov, “Development of compositionally modulated multilayer Zn–Ni deposits as replacement for cadmium”, *Surface and Coatings Technology*, Vol 201, 7896–7904 (2007)
- [59] A. Conde, M.A. Arenas, J.J. de Damborenea, “Electrodeposition of Zn-Ni coatings as Cd replacement for corrosion protection of high strength steel”, *Corrosion Science*, Vol 53, 1489–1497 (2011)
- [60] K.R. Sriraman, S. Brahim, J.A. Szpunar, J.H. Osborne, S. Yue, “Characterization of corrosion resistance of electrodeposited Zn–Ni, Zn and Cd coatings”, *Electrochimica Acta*, Vol 105, 314–323 (2013)

- [61] N. Miura, T. Saito, T. Kanamaru, Y. Shindo, Y. Kitazawa, “Development of new corrosion-resistant steel sheets for automobiles”, Transactions of the Iron and Steel Institute of Japan, Vol 23, 913-922 (1966)
- [62] N. Lotfi, M. Aliofkhaezai, H. Rahmani, G. Barati Darband, “Zinc–Nickel Alloy Electrodeposition: Characterization, Properties, Multilayers and Composites”, Protection of Metals and Physical Chemistry of Surfaces, Vol 54, 1102–1140 (2018)
- [63] H. Okamoto, “Ni-Zn (Nickel-Zinc)”, Journal of Phase Equilibria and Diffusion, Vol 34, 153 (2013)
- [64] L. Felloni, R. Fratesi, E. Quadrini, G. Roventi, “Electrodeposition of zinc-nickel alloys from chloride solution”, Journal of Applied Electrochemistry, Vol 17, 574-582 (1987)
- [65] S. Rajagopalan, S. Brahimi, S. Yue, “Characterization of Hydrogen Permeability in Zn, Zn-Ni, Cd and Cd-Ti Coated Steel”, International Hydrogen Conference (IHC 2012): Hydrogen-Materials Interactions. B.P. Somerday, P. Sofronis Eds. ASME Press, 191-198 (2014)
- [66] O. Barrera, D. Bombac, Y. Chen, “Understanding and mitigating hydrogen embrittlement of steels: a review of experimental, modelling and design progress from atomistic to continuum”, Journal of Materials Science, Vol 53, 6251–6290 (2018)
- [67] M.I. Luppó, J. Ovejero-Garcia, “The influence of microstructure on the trapping and diffusion of hydrogen in a low carbon steel”, Corrosion Science, Vol 32, 1125–1136 (1991)
- [68] ASTM-F1941-00 F1941-00 “Standard specification for electrodeposited coatings on threaded fasteners (Unified Inch Screw Threads (UN/UNR))”, ASTM 20 International, West Conshohocken, PA, 19428-2959, (2006)
- [69] S. Trollst, H. Hoche, M. Oechsner, “Influence of the microstructure of Zn–Ni coatings on hydrogen effusion characteristics”, Journal of Applied Electrochemistry, Vol 50, 935-942 (2020)
- [70] D. Figueroa, M.J. Robinson, “The effects of sacrificial coatings on hydrogen embrittlement and re-embrittlement of ultra-high strength steels”, Corrosion Science, Vol 50, 1066–1079 (2008)

- [71] S. Rajagopalan, S. Brahim, J. Szpunar, S. Yue, “Hydrogen embrittlement of Zn-, Zn–Ni-, and Cd-coated high strength steel”, *Journal of Applied Electrochemistry*, Vol 43, 441-451 (2013)
- [72] “ASTM-G148-97 Standard practice for evaluation of hydrogen uptake, permeation, and transport in metals by an electrochemical Technique”, ASTM International, West Conshohocken, PA, USA (2011)
- [73] M.A.V. Devanathan, Z. Stachurski, “The adsorption and diffusion of electrolytic hydrogen in palladium”, *Proceedings of the Royal Society of London*, Vol 270, 90–102 (1962)
- [74] M.J. Carr, M.J. Robinson, “The effects of zinc alloy electroplating on the hydrogen embrittlement of high strength steels”, *Transactions of the Institute of Metal Finishing*, Vol 73, 58-64 (1995)
- [75] S. Ghaziof, W. Gao, “Electrodeposition of single gamma phased Zn–Ni alloy coatings from additive-free acidic bath”, *Applied Surface Science*, Vol 311, 635-642 (2014)
- [76] J. Bellemare, S. Laliberté-Riverin, D. Ménard, M. Brochu, F. Sirois, “Coating density as the key factor behind hydrogen embrittlement of cadmium-plated 4340 steel”, *Journal of Applied Electrochemistry*, Vol 50, 1045–1058 (2020)
- [77] E.M.K. Hillier, M.J. Robinson, “Hydrogen embrittlement of high strength steel electroplated with zinc-cobalt alloys”, *Corrosion Science*, Vol 46, 715-727 (2004)
- [78] J.K. Dennis, D. Jones, “Brush plating”, *Surface Technology*, Vol 12, 57-73 (1981)
- [79] J.W. Dini, “Brush plating: recent property data”, *Metal Finishing*, Vol 95, 90-93 (1997)
- [80] B. Wu, B. Xu, B. Zhang, X. Jing, C. Liu, “Automatic brush plating: an update on brush plating”, *Materials Letters*, Vol 60, 1673-1677 (2006)
- [81] B. Wu, B. Xu, B. Zhang, Y. Lu, “Preparation and properties of Ni/nano- Al_2O_3 composite coatings by automatic brush plating”, *Surface and Coatings Technology*, Vol 201, 6933-6939 (2007)
- [82] B. Wu, B. Xu, B. Zhang, S. Dong, “The effects of parameters on the mechanical properties of Ni-based coatings prepared by automatic brush plating technology”, *Surface and Coatings Technology*, 5758-5765 (2007)

- [83] P. Behera, S. Rajagopalan, S. Brahim, C.A. Venturella, S.P. Gaydos, R.J. Straw, S. Yue, “Effect of brush plating process variables on the microstructures of Cd and ZnNi coatings and hydrogen embrittlement”, *Surface and Coatings Technology*, Vol 417, 127181 (2021)
- [84] “Steel, Bars, Forgings, and Tubing 0.80Cr - 1.8Ni - 0.25Mo (0.38 - 0.43C) (SAE 4340)” SAE AMS 6415, SAE International (2016)
- [85] “Stress Relief of Steel Parts”, SAE AMS 2759/11A, SAE International (2018)
- [86] K.R. Murali, P. Muthusamy, A. Panneerselvam, “Characteristics of brush plated copper indium telluride films”, *Journal of Materials Science: Materials in Electronics*, Vol 24, 3412–3417 (2013)
- [87] M. Faraday, “On electrical decomposition”, *Philosophical Transactions of the Royal Society*, Vol 124, 77-122 (1834)
- [88] B. Des, F. Walsh, “Applications of Faraday’s laws of electrolysis in metal finishing” *Transactions of the Institute of Metal Finishing*, Vol 69, 158-162 (1991)
- [89] A.M. Rashid, A. Amadeh, “The effect of current density on the grain size of electrodeposited nanocrystalline nickel coatings”, *Surface and Coatings Technology*, Vol 202, 3772-3776 (2008)
- [90] C. Sherwin, S. Bhat, S.P. Hebbar, “Effects of Current Density on Surface Morphology and Coating Thickness of Nickel Plating on Copper Surface”, *Turkish Journal of Computer and Mathematics Education*, Vol 12, 79-83 (2021)
- [91] M. Barsanti, M. Beghini, F. Frascioni, R. Ishak, B.D. Monelli, R. Valentini, “Experimental study of hydrogen embrittlement in Maraging steels”, *Procedia Structural integrity*, Vol 8, 501-508 (2017)
- [92] J. Bellemare, S. Laliberté-Riverin, D. Ménard, M. Brochu, F. Sirois, “Subtleties behind hydrogen embrittlement of cadmium-plated 4340 steel revealed by thermal desorption spectroscopy and sustained-load tests”, *Metallurgical and Materials Transactions A*, Vol 51A, 3054–3065 (2020)